Cenozoic evolution of the Tripolitza carbonate platform in the Tethyan realm: new age constraints on deposition, diagenesis, metamorphism and nappe emplacement based on U-Pb and Rb-Sr dating (External Hellenides, Crete)

T. Klein[1] , G. Zulauf[2] , D. Evans[3] , A. Gerdes[3], J. Glodny[4], F. Heidelbach[5], F. Kirst[2], J. Linckens[6], W. Müller[3], E. Özcan[7], R. Petschick[2] and P. Xypolias[8]

[1]Wintershall Dea AG, Friedrich-Ebert Strasse 160, 34119, Kassel, Germany; [2]Institut für Geowissenschaften, Goethe-Universität Frankfurt a.M., Altenhöferallee 1, D-60438, Frankfurt a.M., Germany; [3]Frankfurt Isotope and Element Research Center (FIERCE), Goethe-Universität Frankfurt a.M., Altenhöferallee 1, D-60438, Frankfurt a.M., Germany; [4]Helmholtz-Zentrum Potsdam, Deutsches GeoForschungsZentrum GFZ, Telegrafenberg, D-14473 Potsdam, Germany; [5]Universität Bayreuth, Bayerisches Geoinstitut (BGI), Universitätsstr. 30, D-95447, Bayreuth, Germany; [6]Tata Steel, R&D, Microstructural and Surface Characterization, 1970 CA, Ijmuiden, The Netherlands; [7]Department of Geological Engineering, Faculty of Mines, İstanbul Technical University, İstanbul, Turkey and [8]Department of Geology, University of Patras, Patras, Greece

Abstract

We present kinematic, radiometric, geochemical and PT data, which help to constrain the tectonometamorphic evolution of the Tripolitza Unit (TPU). The age of both the metamorphic peak ($P = 0.4 \pm 0.2$ GPa, $T =$ ca. 310 °C) and top-to-the WNW mylonitic thrusting, attributed to the emplacement of the hanging Pindos nappe, has been constrained at 19 ±2.5 Ma using Rb-Sr on synkinematic white mica of a basal mylonite of NW Crete. This early tectonic event is also documented by the oldest generation of veins, which cut through less metamorphic ($T = 240 \pm15$ °C) late Bartonian/Priabonian *Nummulite* limestone exposed as olistolith in TPU flysch of central Crete. Calcite of these veins yielded a similar U-Pb age at 20 ±6 Ma. U-Pb dating of matrix calcite, on the other hand, reflect the time of sedimentation (38.4 ±5.7 Ma and 37.6 ±1.2 Ma), which is in line with the faunal content of the black limestone. Geochemical data and U-Pb calcite ages of fibres of the *Nummulite* test (32.3 ±3.1 Ma and 34.6 ±0.9 Ma) suggest unexpected pseudomorphic fibre replacement during late Priabonian/early Rupelian diagenesis. Additional calcite veins, which developed at ca. 10–11 and 7 – 9 Ma (U-Pb on calcite), are attributed to top-to-the S thrusting and subsequent extension, respectively. The resulting anticlockwise rotation of the shortening direction within the TPU from WNW-ESE at ca. 20 Ma to N-S at ca. 10 Ma has significant implications for the geodynamic evolution of the External Hellenides.

1. Introduction

Several platform carbonate sequences that formed in the Tethyan realm have experienced the entire tectonic spectrum of the Wilson cycle, from rifting to collision, and have exerted fundamental control on the architecture of the Alpine orogeny. Therefore, any tectonic interpretation of the regional setting is critically dependent on knowing the provenance, the age and the tectonometamorphic evolution of the carbonate sequences. The challenge lies in retrieving this crucial information from monotonous carbonate rocks using radiometric techniques. That is because, detrital zircons and mineral phases, which can be used for provenance analysis and dating of metamorphism, respectively, are lacking or are very rare in platform carbonate rocks. The mildly metamorphosed Tethyan platform carbonates of the Tripolitza Unit (TPU) can be regarded as a case example where radiometric analyses have been successfully performed.

The TPU belongs to the Alpine nappe stack of the External Hellenides and consists of Triassic to Eocene platform carbonates succeeded by Eocene/Oligocene flysch (Creutzburg & Seidel, 1975; Bonneau & Karakitsios, 1979; Fytrolakis & Antoniou, 1998; Zambetakis-Lekkas *et al.* 1998). The carbonate platform is considered to be part of the northern passive margin of the Mesozoic ocean situated between the Pindos basin in the north and the Neotethyan realm in the south (e.g. Robertson, 2006, 2012; Stampfli & Kozur, 2006). During Alpine subduction and

collision, the rocks of the TPU were deformed and metamorphosed (Klein *et al.* 2012, and references therein).

Although the TPU is a major component of the External Hellenides extending along strike over 600 km, our knowledge about its provenance, age, metamorphism and tectonic evolution is still poor: (1) The provenance and Mesozoic/early Cenozoic position of the TPU platform is only poorly constrained because detrital zircons have not been found in the (meta)carbonates so far. (2) The depositional age of large parts of the (meta) carbonates is unknown, as fossils are either lacking or are destroyed by deformation and metamorphism. (3) The age and type of Alpine metamorphism have yet not been determined because of the lack of metamorphic index minerals and mineral phases, which can be used for radiometric age dating. (4) The kinematics during the emplacement of the TPU on top of the deeper nappes (thrust nappe emplacement vs. extensional detachment) is still intensely disputed (e.g. Fassoulas *et al.* 1994; Jolivet *et al.* 1996; Zulauf *et al.* 2002; Chatzaras *et al.* 2006; van Hinsbergen & Meulenkamp, 2006; Xypolias & Kokkalas, 2006; Klein *et al.* 2008, 2012; Craddock *et al.* 2009; Papanikolaou & Vassilakis, 2010; Ring & Yngwe, 2018, Grasemann *et al.* 2019). (5) The age of the post-metamorphic brittle deformation of the Tripolitza rocks is largely unknown.

In this study, we seek to shed light on these issues and challenges using a spectrum of analytical techniques coupled with field data. The youngest limy beds of the TPU are Upper Eocene black (meta)limestones, which include *Nummulites* and other large benthic foraminifera (LBF) in rock-forming amounts. As the chemical and isotopic composition of foraminiferal tests reflects the physicochemical properties of the seawater, it can be used as so-called proxies. For this reason, *Nummulites* and nummulitids have been used increasingly in geochemical studies (e.g. Wefer & Berger 1980; Purton & Brasier 1999; Evans *et al.* 2013, 2018). The calcite of the test may include uranium as trace element, and the U/Ca ratios can be used as a proxy for seawater uranium (Russell *et al.* 1994) and carbonate ion concentration (Raitzsch *et al.* 2011; Keul *et al.* 2013). The U/Ca ratio of foraminiferal coatings may serve as an ocean redox chemistry proxy (Boiteau *et al.* 2012).

Apart from nummulitids, the middle-upper Eocene carbonates of the Neotethys realm contain orthophragminids, alveolinids and rotaliids, which have been frequently used for biostratigraphic studies (e.g. Schaub 1981; Serra-Kiel *et al.* 1998; BouDagher-Fadel, 2008; Less et al, 2008; Özcan *et al.* 2010, 2016a, 2016b; Cotton & Pearson, 2011; Papazzoni *et al.* 2017; Özcan *et al.* 2019, and references therein). Such microfossils have also been found in the studied samples and could be used for constraining the biostratigraphic age of the black (meta)limestones, which will be compared with the U-Pb age obtained from calcite fibres of the *Nummulite* tests. As U^{4+} has been shown to replace Ca^{2+} in the calcite lattice (Kelly *et al.* 2003, 2006), the age of calcite formation can be dated using the U-Pb method (e.g. Jahn *et al.* 1990; Jahn & Cuvellier, 1994; Smith *et al.* 1994; Israelson *et al.* 1996; Richards *et al.* 1998; Sturchio *et al.* 1998; Rasbury & Cole, 2009; Godeau *et al.* 2018).

The U-Pb data of Nummulite calcite are less distinct because of the following reasons. (1) It is possible that in biomineralization uranium is preferentially concentrated during the transport of dissolved inorganic carbon (DIC). As foraminifers uptake DIC, uranyl–DIC complexes may also be incorporated with calcifying fluid as part of this process (Weremeichik *et al.* 2017). In this case, the U-Pb age of the calcite would reflect the age of the foraminifer. (2) The primary calcite of the Nummulite test is replaced by secondary calcite during diagenesis revealing that the U-Pb age yields the time of diagenesis. (3) In cases of metamorphic rocks,

primary calcite could have been replaced by secondary calcite during the metamorphic overprint. Thus, the U-Pb age reflects the time of metamorphism.

While both a low-Mg and high-Mg original mineralogy of the *Nummulites* has been argued for, recent geochemical and spectroscopic analysis of exceptionally well-preserved Eocene samples from globally distributed locations has demonstrated that, like their modern relatives, these foraminifera were originally made of high-Mg calcite (Evans *et al.* 2013; Cotton *et al.* 2020). The instability of high-Mg calcite means that these foraminifera readily change to low-Mg calcite during (early) diagenesis, which holds particularly for carbonates affected by metamorphism. In order to determine if the calcite of the *Nummulite*s tests utilized here are of primary or secondary origin, we carried out geochemical and electron backscattered diffraction analyses (EBSD) analyses. As the large uranyl ion does not rapidly diffuse out of the calcite lattice, it could be retained during replacement, meaning that U-Pb dating of secondary calcite derived from primary calcite should be possible (Kelly *et al.* 2003; 2006). However, Pb loss may occur during 'recrystallization' (Smith *et al.* 1994).

In recent years, U-Pb dating of calcite mineralization, using the laser ablation inductively coupled plasma mass spectrometry technique (LA-ICP-MS), turned out as a novel approach in obtaining precise ages of calcite-bearing faults and veins (Rittner & Müller, 2011; Coogan *et al.* 2016; Ring & Gerdes, 2016; Roberts & Walker, 2016; Burisch *et al.* 2017; Nuriel *et al.* 2017; Hansman *et al.* 2018). Thus, apart from dating the *Nummulite* tests, we applied this method also to calcite, which precipitated in tectonic veins of the (meta)carbonates of the TPU.

Finally, syn-kinematic white mica that grew in a ductile shear zone of the basal marbles of the TPU allow us to constrain the type and age of metamorphism using the Si content in white mica and the Rb-Sr method of dating, respectively. The deformation mechanisms in calcite and the kinematics during shearing were revealed using microscopic and EBSD data. EBSD data have further been obtained from calcite fibres of Nummulite tests to unravel their origin (pristine or diagenetic).

The new results presented in this contribution shed light on the age of deposition, diagenesis, metamorphism and brittle deformation of TPU rocks and thus help to improve our understanding of the Alpine geodynamic evolution of the External Hellenides.

2. Geological setting

The TPU is exposed on Crete (Fig. 1) as well as on the Peloponnesus, Kythira and Rhodes. It consists of late Triassic to late Eocene neritic (meta)limestones and dolomites, which are overlain by late Eocene (Priabonian) to Oligocene flysch (Renz, 1913, 1955; Creutzburg & Seidel, 1975; Thorbecke, 1976; Tsaila-Monopolis, 1977; Seidel & Wachendorf, 1986; Manutsoglu *et al.* 1993; Zambetakis-Lekkas *et al.* 1998). Some of the (meta) carbonates at the base of the TPU show a Ladinian-Carnian fauna (Haude, 1989), which predates the age of the youngest sediments of the Permian to Triassic Tyros Unit underneath. Apart from the Tyros Unit, the rocks of the TPU have been thrust on top of Neogene sediments (Kokkalas and Doutsos, 2001; Klein *et al.* 2012). In Crete and the Peloponnesus, the thrust contact may cut considerably down-section until the Plattenkalk Unit, which is the structurally deepest constituent of the Cretan nappe stack (Fig. 1). The TPU itself is tectonically overlain by the Triassic to Paleogene rocks of the Pindos and the Uppermost Unit (Fig. 1). Both the
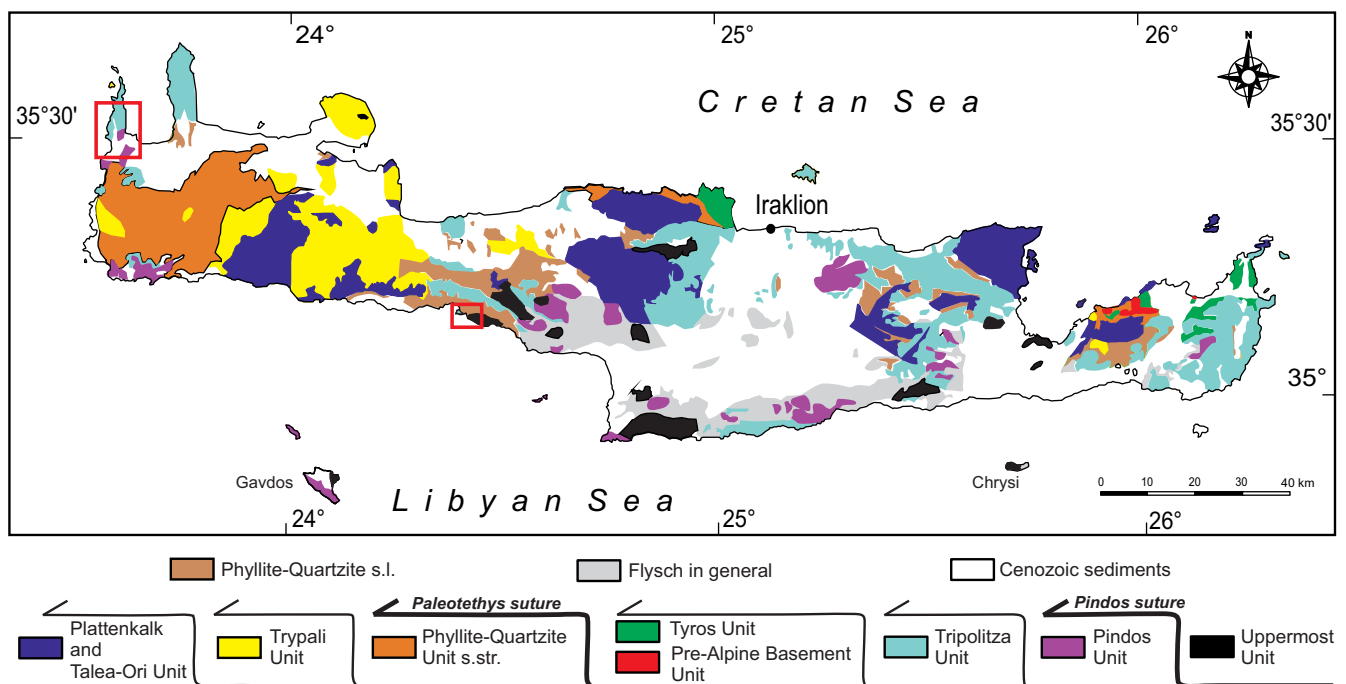
Figure 1. (Colour online) Geological map of Crete (modified after Zulauf *et al.* 2018, and references therein) showing study areas at the southern and western coast of Crete (red insets).

Tripolitza limestone and flysch underwent Alpine deformation and metamorphism. Conodont alteration (Epstein *et al.* 1977, as cited in Bonneau, 1984), illite crystallinity (IC) (Feldhoff *et al.* 1991; Klein *et al.* 2012), vitrinite reflectance (Feldhoff *et al.* 1993), and CM geothermometry (Rahl *et al.* 2005) of Tripolitza (meta) limestones indicate metamorphism of very low grade to lower epizone ($T = 240–320$ °C). Fission-track dating of apatite of the TPU yielded 17.5 ±2.5 Ma (Thomson *et al.* 1999) and 15–17 Ma (Rahl *et al.* 2005).

3. Methods

The tectonic structures and the deformation microstructures as well as the type, structure and alteration of microfossils (largely *Nummulites*) of the Tripolitza rocks were analysed using a petrographic microscope. Three samples were collected in the Falasarna area of NW Crete, and five samples were collected in the Damnoni area east of Plakias. Those samples, which were investigated and described in detail are listed in Table S3 Supplement. Constituent minerals have further been determined from all of the analysed samples using semi-quantitative *X-ray powder diffraction (XRD)*. Dry samples were pulverized dry in an agate mortar and 0.5 g of each sample measured using a Panalytical X'Pert Pro diffractometer. Evaluation of the data was performed using the software X'Pert HighScore Plus and MacDiff to obtain semi-quantitative mineral contents of the studied samples.

To reveal the crystallographic preferred orientation (CPO) of calcite fibres in *Nummulite* tests and of calcite crystals of ductile shear zones, the samples were examined using *EBSD* analysis. After performing petrographic analyses, thin sections were embedded in epoxy resin and then polished with colloidal silica on a vibratory polisher (SYTON method). Thin sections were coated with a thin layer of carbon and surrounded with a thin copper band in order to minimize ionic charging. EBSD analyses were conducted using a JEOL JSM 6490 scanning electron microscope (SEM) at Goethe University Frankfurt a.M. equipped with a HKL Nordlys EBSD detector. Acceleration voltage for the measurements was 15 kV, beam current was ~8 nA, and the working distance is between 17 and 20 mm. EBSD patterns were indexed using the HKL Technology CHANNEL 5 software (Schmidt & Olesen 1989). Only EBSD measurements with a mean angular deviation (MAD) of <1.3 were accepted and recorded. Maps were generated using a step size of 0.5 μm.

EBSD analysis of the basal TPU mylonite was performed on SYTON polished and carbon-coated rock specimens (same face as thin sections) using a Leo (Zeiss) Gemini 1530 SEM equipped with a thermionic emission gun (Schottky emitter) and forescatter electron (FSE) detector at the University of Bayreuth. Acceleration voltage was 20 kV, the beam current was about 4 nA and the working distance was 20 mm. The EBSD camera and software as well as analytical conditions for EBSD patterns were the same as above. Calculated misorientation angles are minimum angles. Only calcite was analysed.

For *Rb-Sr dating,* Rb and Sr concentrations of white mica were determined by isotope dilution using mixed ^{87}Rb–^{84}Sr spikes. Rb and Sr isotope ratios were determined on a VG-Sector 54 multicollector Thermal Ionization Mass Spectrometry (TIMS) instrument (GeoForschungsZentrum, Potsdam) in dynamic mode. The value obtained for ^{87}Sr/^{86}Sr of the National Bureau of Standards (NBS) Standard Reference Material (SRM) 987 was 0.710268 ±0.000015 (n = 19). The observed ratios of Rb analyses were corrected for 0.25% per amu mass fractionation. Total procedural blanks were consistently <0.15 ng for both Rb and Sr. Due to highly variable blank values, no useful blank correction was applicable. Isochron parameters were calculated using the Isoplot/ Ex program of Ludwig (1999). Standard errors, as derived from replicate analyses of spiked white mica samples of ±0.005% for ^{87}Sr/^{86}Sr ratios and of ±1.5% for Rb-Sr ratios were applied in isochron age calculations. Individual analytical errors were generally smaller than these values.

Prerequisites to obtain robust *U-Pb ages of calcite* and carbonates are (1) a closed isotopic system, (2) a homogeneous initial ('common') Pb composition, and (3) a sufficient spread in U-Pb data points on Tera-Wasserburg concordia or on isochron plots. Because of low U and radiogenic Pb concentrations in carbonates, large spot sizes are required during U-Pb LA-ICP-MS analysis.

Uranium-Pb ages of calcite were acquired in situ in polished thin sections using a ThermoScientific Element XR ICP-MS that is coupled to a RESOlution (Resonetics) 193 nM ArF Excimer laser (CompexPro 102, Coherent) equipped with a two-volume ablation cell (Laurin Technic, Australia). Analytical details are summarized in Supplemantary Table S1a. Raw data were corrected offline using an in-house MS Excel©spread sheet program (Gerdes & Zeh, 2009). The U-Pb data of calcite are plotted in Tera-Wasserburg diagrams.

Microprobe analyses of white mica were performed using a JEOL electron microprobe (JXA-8200) at the Mineralogical Department of Erlangen University. Calibration was carried out using natural and synthetic oxide and metallic standards from P&H Developments Ltd. The acceleration voltage has been set to 15 kV. Measurements were acquired utilizing a defocused electron beam of ca. 6 µm diameter and relatively low beam currents of ca. 10 nA in order to mitigate thermal heating and potential destruction of the polished white mica surfaces. Counting times were 20 sec. (peak intensity) and 10 sec. (upper and lower background intensities), respectively. ZAF corrections were applied.

Spatially resolved trace element analysis of the nummulitic limestone was performed by laser ablation ICP-MS in the FIERCE laboratory, Goethe-Universität Frankfurt, in order to assess the geochemical preservation of these sediments. The hardware set-up was the same as that described in relation to the U-Pb dating above. For trace element analysis, ablation took place in a He atmosphere with 950 ml/min Ar admixed into the inner volume ablation cell, with 4 ml/min N_2 used as an additional diatomic gas to improve sensitivity, added downstream of the ablation cell. To maximize vertical spatial resolution, thin sections containing *Nummulites*, calcite matrix and calcite veins were analysed via slow depth profiling using a beam diameter of 44 µm and a laser repetition rate of 2 Hz. A 'squid' signal smoothing device was used to avoid spectral skew under these ablation conditions (Müller *et al.* 2009). The ICP-MS was run in 'triple' collection mode, with automatic switching between counting, analogue and Faraday cup detection methods. The instrument was equipped with a Ni jet sample cone and Ni H skimmer cone and tuned for maximum sensitivity whilst ensuring robust plasma conditions (Fietzke & Frische, 2016) with 1300 W RF power, by ensuring Th/U was between 0.95 and 1.00, ThO^+/Th^+ <0.5% and Ca^{2+}/Ca^+ (m/z 22/44) below 2%. The monitored masses were ^{11}B, ^{23}Na, ^{24}Mg, ^{25}Mg, ^{27}Al, ^{55}Mn, ^{56}Fe, ^{66}Zn, ^{88}Sr, ^{89}Y, ^{138}Ba, ^{146}Nd and ^{238}U. The ICP-MS was run in medium resolution to resolve the polyatomic interferences on ^{27}Al, ^{55}Mn and ^{56}Fe.

Data reduction followed standard procedures using an in-house Matlab script (Longerich *et al.* 1996; Evans & Müller, 2018), using ^{44}Ca as the internal standard and NIST SRM612 as the calibration standard, except in the case of Mg, for which NIST SRM610 was used because it has a [Mg] much closer to that of the samples and is more homogenous with respect to this element (Evans & Müller, 2018). We use the preferred NIST values of Jochum *et al.* (2011) in all cases except for Mg, as discussed in detail elsewhere (Evans & Müller, 2018). In order to assess accuracy and precision of the trace

element data, five different carbonate and glass standards were ablated in the same session as the samples using identical ablation and plasma conditions. Specifically, the carbonate nano pellet standards JCp, JCt and MACS-3 (Garbe-Schönberg & Müller 2014) and the MPI-DING glasses GOR132-G and GOR128-G (Jochum *et al.* 2006) were analysed 2–5 times each. Because we are interested in the broad trace element composition of the samples discussed here rather than obtaining the most precise and accurate results possible for any single trace element, we report accuracy based on the mean measured values compared to the reported values from all five standards, as this avoids bias associated with the reported value of any individual standard (Evans & Müller, 2018). Determined in this way, accuracy was <1% for Mg/Ca, Al/Ca, Sr/Ca, and U/Ca, <5% for B/Ca, Na/Ca, Fe/Ca, Y/Ca, and Nd/Ca, and <10% for Ba/Ca. Mn/Ca and Zn/Ca accuracy strongly depends on concentration. Mn/Ca accuracy was <1% based on JCp, GOR-132G and GOR128-G (Mn/Ca = 1–22 mmol/mol) but substantially worse (~100%) at concentrations an order of magnitude lower than this (JCt and MACS-3 Mn/Ca = ~4–10 µmol/mol), although we note that the issue may equally be the extent to which the Mn concentration of these standards is well characterized. Similarly, Zn/Ca accuracy was 19% based on JCp, GOR132-G and GOR128-G (Zn/Ca = 0.2–1.0 mmol/mol) but much less favourable in the case of JCt and MACS-3 (100–300%, Zn/Ca = 5–8 µmol/mol).

Precision is reported based on the 2SD of repeat measurements of the standard that has a given logarithm of the trace element/Ca ratio closest to that of the logarithm of the sample ratios, on an element-specific basis, as precision strongly depends on the intensity of the ion beam. Assessed in this way, precision was <5% for Mg/Ca, Mn/Ca, Sr/Ca, Y/Ca, and Nd/Ca, <10% for Na/Ca and U/Ca, and <20% for B/Ca, Al/Ca, Fe/Ca, and Ba/Ca. Given the very low Zn/Ca ratios of the samples (~4 µmol/mol), precision assessed using JCt was poor (~250%), although we stress that we do not assign meaning to the specific details of these measurements (see Sec. 4.1.3). All data described here are given in Supplementary Table S2.

4. Results

4.a. Nummulite-*bearing olistolith of Tripolitza wildflysch (Damnoni Bay, central Crete)*

4.a.1. *Composition, biostratigraphic age constraints, structure and deformation microfabrics*

The dark *Nummulite*-bearing (meta)limestone was collected from a large olistolith embedded in Tripolitza wildflysch at Damnoni Bay (Figs. 2, 3a; Supplementary Table S3). Apart from this type, there are also large olistoliths, which consist of *Hippuritoida*-bearing Upper Cretaceous (meta)limestone also derived from the upper part of the TPU (meta)carbonates (Fig. 2; Karakitsios, 1982).

XRD analyses of the dark (meta)limestone revealed calcite as the most important phase. Illite and/or white mica have not been found in the 10 Å domain. The amount of phyllosilicates is <5%. *Nummulites* and other LBF are up to 2 cm in size and are best visible on weathered surfaces. Their distribution is not homogeneous throughout the dark (meta)limestone. In some parts the amount of LBF is very high, whereas in other parts the rock is dominated by the black fine-grained limy matrix with only few LBF disseminated therein (Fig. 3b, c). This distribution of LBF, together with the weak shape-preferred orientation of the *Nummulite* tests, reflects bedding.
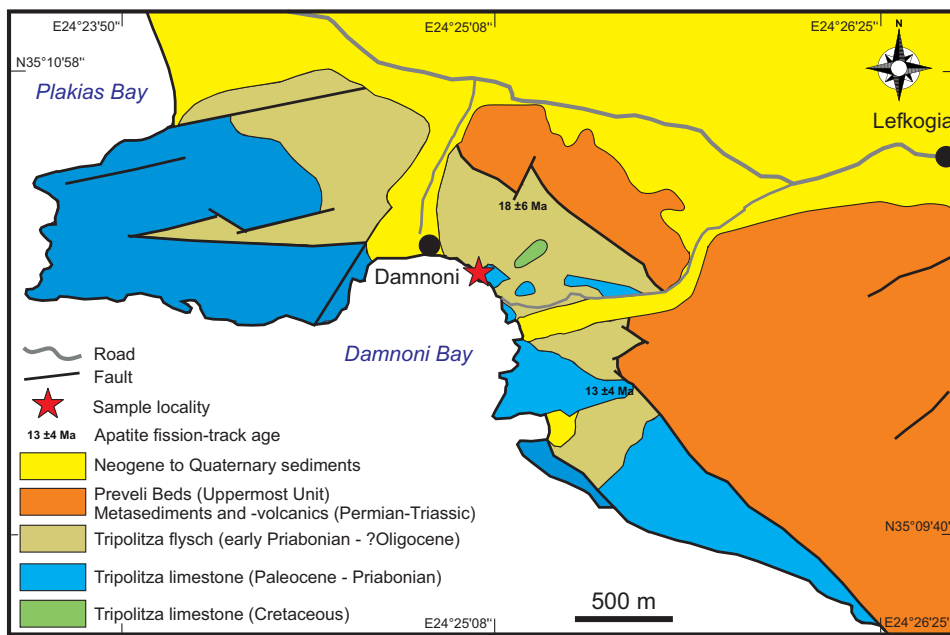
Figure 2. (Colour online) Geological map of study area at Damnoni Bay of central Crete (after Karakitsios, 1982, and new mapping). Apatite fission-track ages after Thomson *et al.* (1999).

Microscopic analyses revealed that apart from the LBF, there are also numerous small foraminifers embedded in the black limy matrix (Fig. 4a, b). The size of these foraminifers varies gradually. Using the classification of Dunham (1962), the black (meta) limestone turned out to be a bioclast (meta)wackestone to (meta) packstone. Apart from a large number of reticulate nummulitids, there are ?lepidocyclinids, orthophragminids and operculinids, some of which may belong to *Heterostegina* (see also Özcan *et al.* 2016a, 2016b). The presence of *Pellatispira madaraszi* (Fig. 4c), which appears at latest Bartonian and persists in the Priabonian (Özcan *et al.* 2019), constrains the age of the rock.

Most of the *Nummulites* are unspoiled concerning their shape. Pieces of fractured and broken *Nummulites* are rare but may be enriched in distinct domains. The tests of the *Nummulites* consist of radial calcite fibres, which are up to 0.5 mm long and 10–15 μm in diameter (Fig. 4d, e). Some of the *Nummulites'* tests include heavy minerals, which are up to 50 μm in size (Fig. 4e, f). The majority of these heavy minerals are colourless and euhedral with a shape that fits well to that of zircon.

Alpine deformation under very low-grade metamorphic conditions was polyphase and accommodated by fracturing and solution-precipitation creep. There is no evidence for dislocation creep and related recrystallization of calcite. The calcite veins of the dark (meta)limestone are up to 1 mm wide. Most of them are syntaxial veins, where calcite grains grew from the margins towards the centre of the vein (Fig. 5a). For this reason, the size of the calcite crystals is commonly much smaller along the margins (up to 50 μm) compared to the central part (coarse blocky grains up to 0.5 mm). Some veins are displaced along younger shear fractures or are cut by younger veins (Fig. 5b). Antitaxial calcite veins are rare (Fig. 5c). In cases where the calcite veins cut through *Nummulites*, their attitude can be deflected by the calcite fibres of the *Nummulite* tests, which acted as a mechanical anisotropy (Fig. 5c). The strong and anisotropic behaviour of the test fibres is also indicated by their twinning (Fig. 5a). Large calcite grains of the veins show straight, thin deformation twins, which belong to type 1 twins according to the classification of Burkhard (1993). Evidence for pressure solution is present in the form of stylolites and strain

caps, which are particularly well developed where *Nummulites* are abutting (Fig. 5d).

4.a.2. Texture of Nummulite calcite based on EBSD analysis

EBSD analyses have been carried out on the tests of large Nummulites of sample 190926-1, which consist of radial calcite fibres as described above. One analysed section of fibres is depicted in the upper part of Fig. 6. The fibres show similar colours, which do not vary along the axes of the fibres. When plotting the EBSD data of the fibres in an equal-area net, they show a strong alignment of crystallographic <c>axes ([0001]) parallel to the long axis of the fibres, whereas other {11–20} result in a girdle that is perpendicular to [0001] (Fig. 6).

4.a.3. Chemical composition of calcite of Nummulite test and veins

In total, nine foraminifera from three different thin sections of samples 190926-1 and 190926-2 were analysed 3–5 times, respectively (32 analyses in total). In two of these thin sections, five calcite veins that cross-cut the foraminifera were analysed for comparison (all data presented here are given in Supplementary Table S2, and location of analysed samples is shown in Fig. 2 and is listed in Supplementary Table S3. Despite the observation that the foraminifera retain even some fine details of the morphological microstructure and the crystallographic orientation of their tests, the composition of these specimens is characterized by almost complete diagenetic overprinting. This is most obvious in their Mg/Ca and Sr/Ca ratios (20.0 ±2.3 and 0.73 ±0.65 mmol/mol, respectively; 2SD variability between specimens), which are characteristic of complete 'recrystallization' of the original high-Mg calcite of *Nummulites*, as discussed in detail in Cotton *et al.* (2020); pristine modern nearest living relatives and exceptionally preserved Eocene *Nummulites* have Mg/Ca ratios of 80–160 mmol/mol and Sr/Ca ratios of 1.8–2.6 mmol/mol. This diagenetic loss of trace elements that substitute for both Ca and CO_3 in the crystal lattice is also clearly visible in the B/Ca ratios of these specimens (19.5 ±6.6 μmol/mol), Na/Ca (0.65 ±0.32 mmol/mol), Zn/Ca (0.5 ±0.5 μmol/mol) and Ba/Ca

Figure 3. (Colour online) Macroscopic views of investigated rocks exposed at the eastern part of Damnoni beach (35°10'23"N, 24°25'05"E). (a) Large olistoliths of Tripolitza limestone embedded in Tripolitza flysch. View is towards the W. (b) Olistolith of dark Nummulite limestone in the foreground. Light olistoliths in the background consist of Rudist-bearing limestone. View is towards the W. (c) Close-up view of the dark Nummulite limestone showing various kinds and sections of Nummulites and of veins filled with calcite. Samples 90926-1 and 90926-2 were collected at this site.

(1.3 ±0.9 μmol/mol), all of which are reduced by a factor of ~2–20 compared to pristine modern and well-preserved fossil material (see Evans *et al.* 2013, 2018; Hauzer *et al.* 2018; Cotton *et al.* 2020). The exception to this diagenetic loss is U/Ca, which is ~5 times higher than in modern nearest living relatives. The lowest concentration proxy trace element (Zn) and elements that are indicative of sediment contamination (Al) or early-stage overgrowths (Mn, Y and Nd) are also present at element/Ca ratios 1–10 times lower than pristine material.

In addition, the comparative analyses of the calcite veins present in the same sections show that the composition of the foraminifera and vein calcite is very similar. While very broad correlations between element/Ca ratios in calcite may be expected because these are governed to a large degree by compatibility, the very similar Na, Mg, Al, Zn, Y, Nd and U/Ca ratios, with the veins being characterized by ±50% of the foraminifera values, strongly support the notion that the composition of these *Nummulites* is explicable through extensive diagenetic replacement. Of the higher concentration trace elements in calcite, only Sr/Ca and Ba/Ca

remain substantially elevated in the foraminifera compared to that of the calcite veins (Sr/Ca = 0.72 ±0.22 and 0.19 ±0.07 mmol/mol in the foraminifera and veins, respectively, Ba/Ca = 1.3 ±0.3 and 0.5 ±0.7 μmol/mol, respectively; uncertainties on mean values are 2SE).

4.a.4. U-Pb ages of calcite included in Nummulite tests and in veins

Calcite of the dark limy matrix (Fig. 7a,b) yielded U-Pb ages at 38.4 ±5.7 Ma and 37.6 ±1.2 Ma (Fig. 8a, b; Supplementary Table S1b). These late Eocene ages should reflect the age of deposition. The calcite fibres of the *Nummulite* tests yielded younger U-Pb ages at 32.3 ±3.1 Ma and 34.6 ±0.9 Ma, which are straddling the Eocene/ Oligocene boundary (Fig. 8c, d). These ages could be related to the diagenetic overprint.

U-Pb dating of vein calcite (Fig. 7) revealed at least three generations of veins, which are different in age even when considering the uncertainties. The oldest generation of veins (vein 3.4, sample 190926-1, Fig. 7b,e) yielded 20.1 ±5.6 Ma (Fig. 9a;
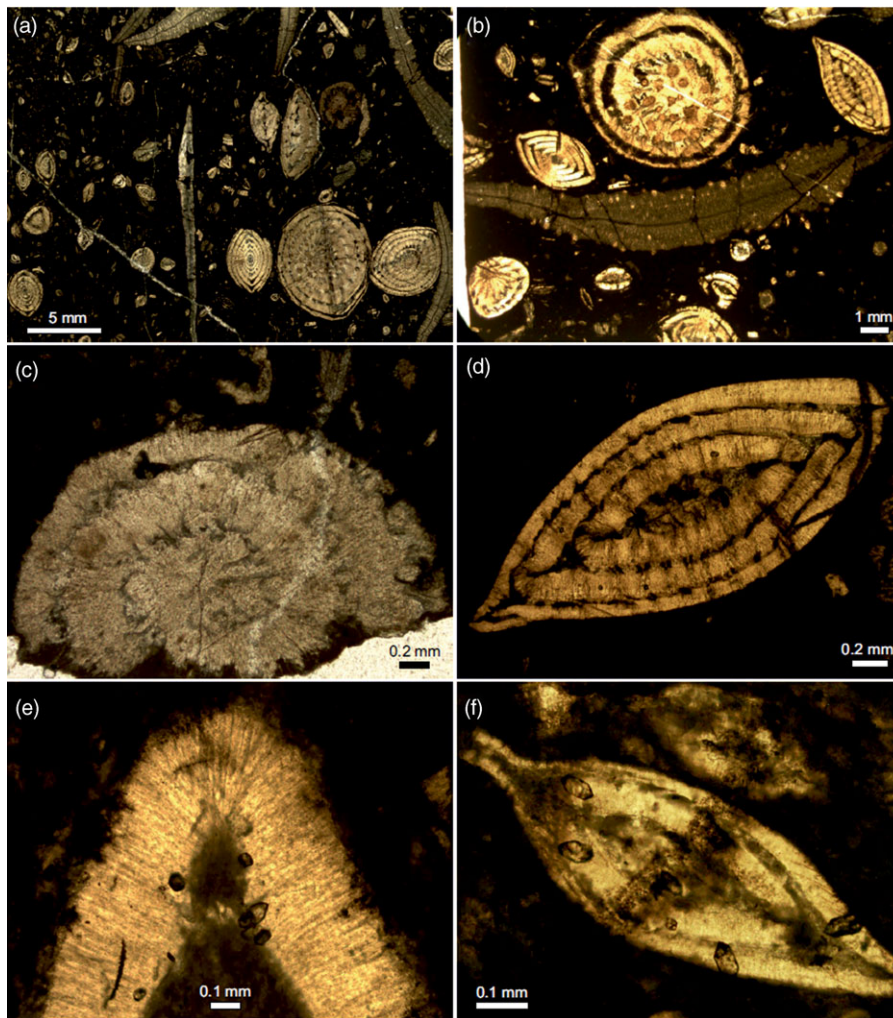
Figure 4. (Colour online) Microphotographs of black Nummulite-bearing marble; parallel polarizers. (a) Overview screen of bioclast nummulitidae lepidocyclinidae (meta) wackestone; younger fractures are filled with calcite (sample 190926-1c). (b) Various sections through Nummulite tests (sample 190926-1b). (c) Pellatispira madaraszi Hantken 1876 (latest Bartonian to Priabonian) (sample 190926-1b). (d) Well preserved shape and calcite fibres of Nummulite test (sample 190926-1b). (e) Test of Nummulite showing radial calcite fibres and tiny inclusions of heavy minerals (probably zircon, which are partly euhedral (sample 190926-1). (f) Nummulite test with inclusions of heavy minerals, largely euhedral zircons (sample 190926-1).

Supplementary Table S1b). Although this early Miocene age has a large uncertainty, it is clearly younger than the ages mentioned above. Secondary calcite fillings of cavities as well as veins 4.1 and 4.2 of sample 190926-2 (Fig. 7a) yielded U-Pb ages at 10.6 ±3.1 Ma, 10.3 ±0.3 Ma and 10.1 ±0.6 Ma (Fig. 9b–d). The youngest generation of veins (veins 3.2 and 3.3 of sample 190926-1, Fig. 7b, d, f) has been dated at 7.9 ±0.5 Ma and 8.8 ±0.5 Ma, respectively (Fig. 9e, f; Supplementary Table S1b).

4.b. Mylonitic shear zone of basal Tripolitza Unit (Falasarna, western Crete)

4.b.1. Structure and microfabrics

A ductile top-to-the WNW shear zone, which cuts through the basal part of Tripolitza marble, was recognized at the western coast of Crete, ca. 1 km north of the ancient Roman harbour Falasarna (sample 020414/7-2, Fig. 10). The shear zone is generally subhorizontal or locally shallowly dipping (Fig. 11a). The shear planes display a distinct WNW-ESE trending stretching lineation defined by elongated calcite aggregates (Figs. 11c; 9a in Klein *et al.*

2012). The drag of a sheared calcite vein and displaced thin calcite veins indicate a top-to-the WNW sense of shear (Fig. 11b,d). Microscopic analysis revealed that the calcite marble is pervasively recrystallized and affected by solution-precipitation creep, which led to dark stylolitic seams. During subsequent ductile deformation, these seams were rearranged and transformed into poorly defined SC fabrics, which seem to verify the macroscopic top-to-the WNW sense of shear (Fig. 11e). The same sense of shear is indicated by asymmetric pressure shadows of calcite behind rigid clasts of albite. Apart from clay and heavy minerals in the dark seams, there is white mica, the long axis of which is aligned parallel to the main stretching direction. As such type of mica has not been observed in the wall rock, a synkinematic growth during ductile shearing is assumed (Fig. 11f).

EBSD analysis of mylonitic marble revealed an asymmetric distribution of the calcite <c>axes ([0001]) in *XZ* sections (Fig. 12a). This asymmetric fabric should result from non-coaxial deformation consistent with the top-to-the WNW shearing described above. However, the texture is weak and not clearly related to a particular intracrystalline slip system of calcite such as
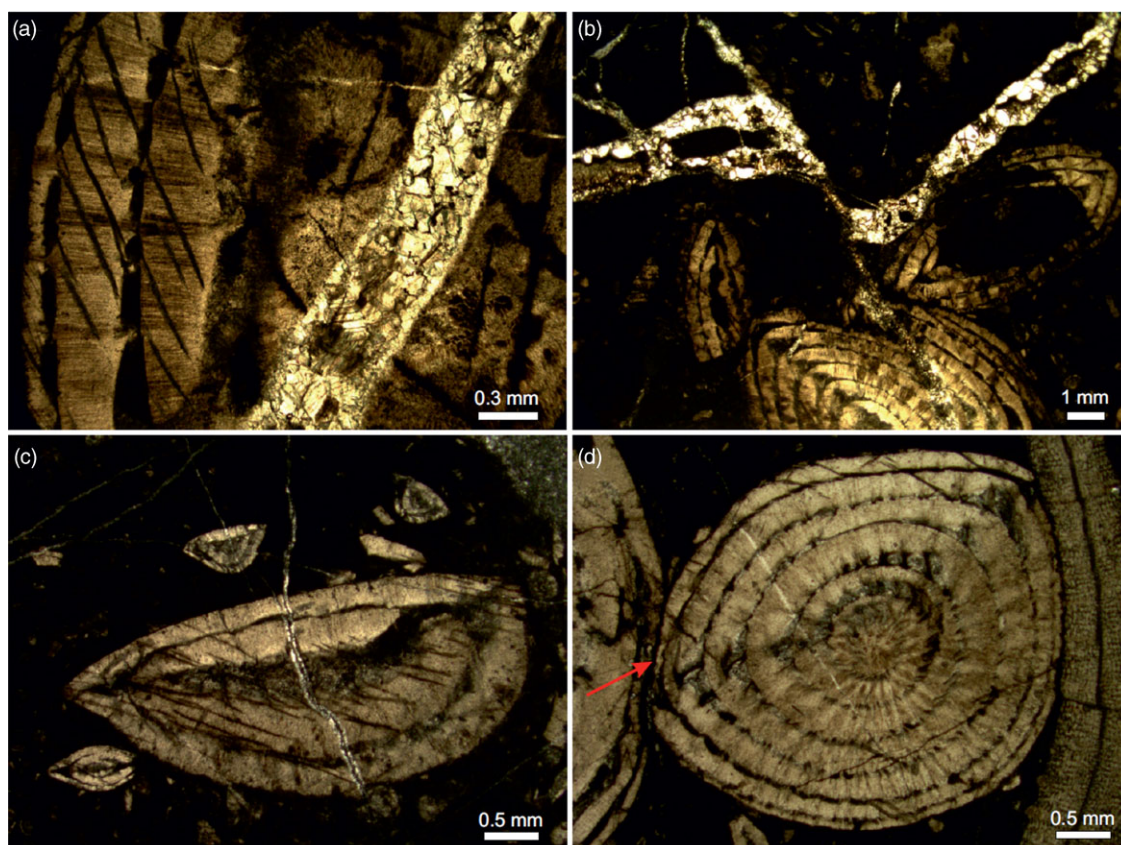
Figure 5. (Colour online) Microphotographs of black Nummulite-bearing marble showing deformation microfabrics of calcite; all under parallel polarizers. (a) Syntaxial calcite vein filled with small grains along the margins and larger blocky grains in the centre. Note that large crystals are twinned. The dark hatching in the Nummulite test (left-hand side) might represent calcite twins (sample 190926-1). (b) Thick vein of calcite includes fragments of wall rock and is displaced by younger discrete shear plane (sample 190926-1c). (c) The attitude of an antiaxial calcite vein (with a median line) is affected by the mechanical anisotropy of the Nummulite-test fibres (sample 190926-1a). (d) Close-up view of Fig. 4a. Evidence for pressure solution at the contact between two Nummulites indicated by red arrow (sample 190926-1c).
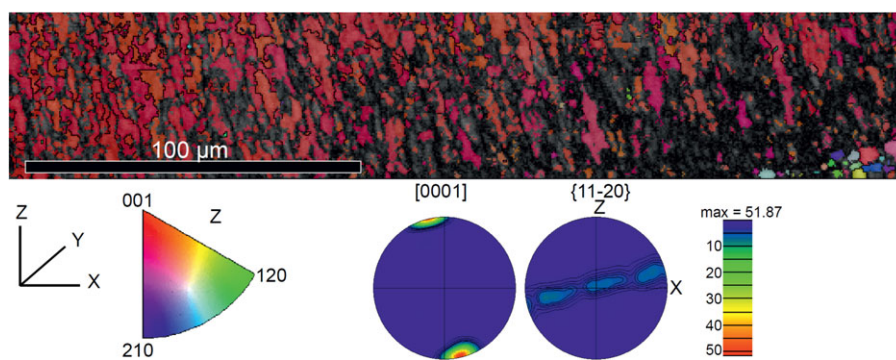

Figure 6. (Colour online) Results of EBSD analyses of calcite fibres belonging to test of Nummulite (sample 190926-1). The fibres display a strong crystallographic preferred orientation, which correlates well with the direction of the fibres. The [0001] direction is parallel to the long axes of the fibres.

r- and f-gliding (e.g. De Bresser & Spiers, 1997). Apart from a distinct amount of subgrain boundaries, most of the calcite boundaries are high angle and thus grain boundaries (Fig. 12b). The presence of subgrains reflects dislocation creep as deformation mechanism. The weak CPO of calcite can be explained by two possible scenarios: (1) overprint of a preexisting statically equilibrated fabric by mylonitic shearing, or (2) overprint of a preexisting CPO of calcite (which resulted from mylonitic shearing) by grain-boundary sliding (GBS) and grain rotation. The second scenario is more appropriate, as mylonitic shearing leads to grain size reduction, which supports GBS and thus the weakening of the older CPO. Notable microstructural criteria indicative for GBS are small (<10 μm) equant grains lacking a strong CPO (e.g. Bestmann & Prior, 2003). Both GBS and dislocation creep, in form of subgrain formation, are fully compatible with the epizonal metamorphic conditions (ca. 310° C) obtained for the Tripolitza rocks exposed near Falasarna (Klein *et al.* 2012). Further details about the kinematics and deformation microfabrics of this shear zone are reported in Klein *et al.* (2006, 2012).

Bent twin lamellae or twinned twins in larger calcite crystals suggest temperatures >200 °C (Burkhard, 1993; Ferrill *et al.* 2004) during deformation stages, which postdate the metamorphic peak.

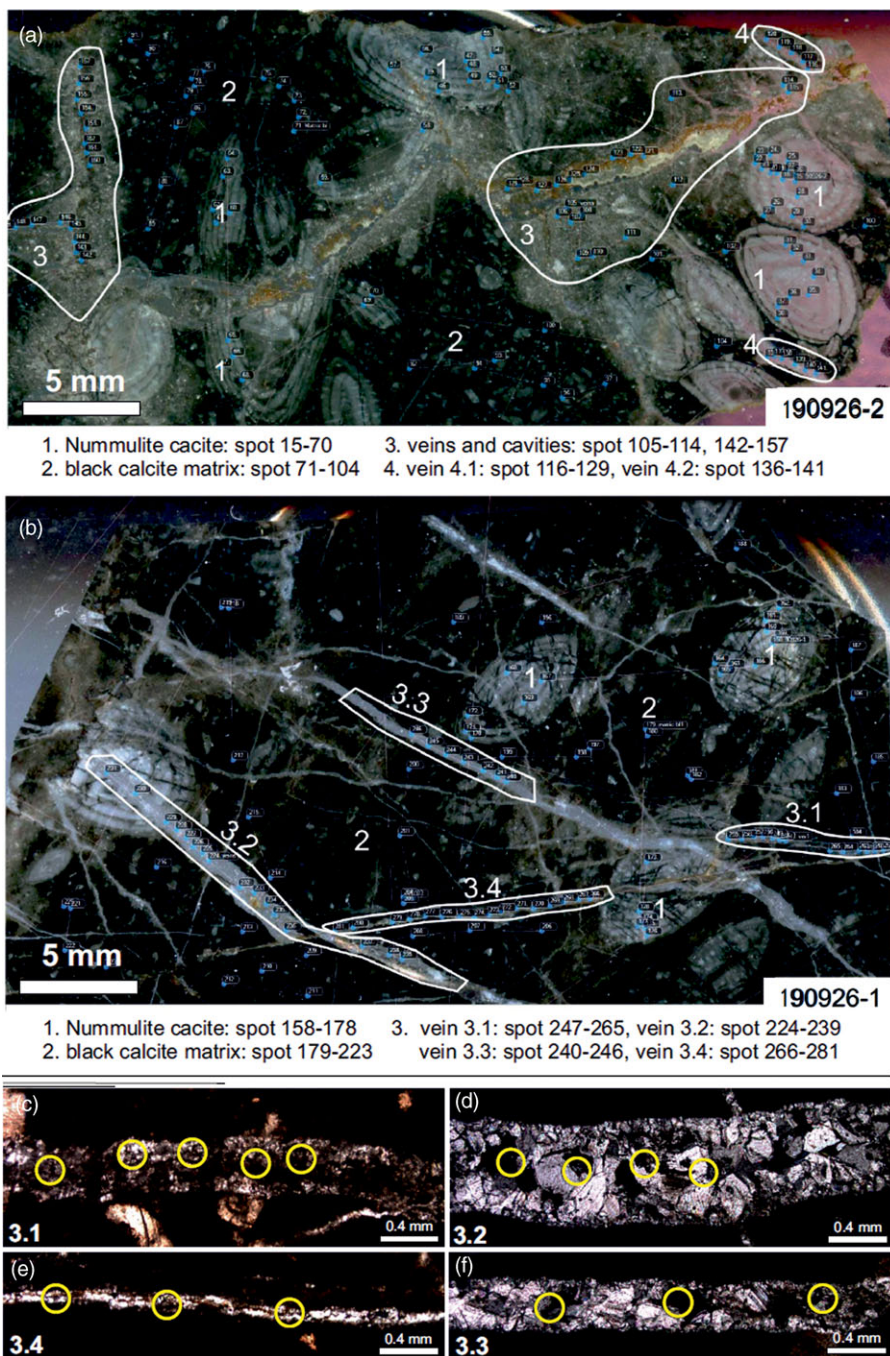1. Nummulite cacite: spot 15-70   3. veins and cavities: spot 105-114, 142-157
2. black calcite matrix: spot 71-104 4. vein 4.1: spot 116-129, vein 4.2: spot 136-141

1. Nummulite cacite: spot 158-178   3. vein 3.1: spot 247-265, vein 3.2: spot 224-239
2. black calcite matrix: spot 179-223 vein 3.3: spot 240-246, vein 3.4: spot 266-281

Figure 7. (Colour online) Microphotographs of black Nummulite-bearing marble showing the areas used for U-Pb dating of calcite and for trace element analyses; parallel polarizers. (a) Sample 190926-2. (b) Sample 190926-1. (c) Close-up view of syntaxial vein 3.1. (d) Close-up view of syntaxial vein 3.2. (e) Close-up view of vein 3.4. (f) Close-up view of syntaxial vein 3.3. Analysed spots are indicated by yellow circles.

4.b.2. Rb-Sr dating and microprobe analysis of white mica

The sample for Rb-Sr dating and microprobe analysis of white mica (020414/7-2) was collected from the ductile shear zone described above. The chemical analysis suggests the white mica to be phengitic in composition with an Si content between 3.2 and 3.3. p.f.u. (Supplementary Table S4). Applying the phengite barometer of Massonne & Schreyer (1987) and Massonne & Szpurka (1997) for a metamorphic temperature of 300–350 °C (see above), these Si values reveal a minimum pressure of 0.2–0.6 GPa (Fig. 13).

The separation of white micas was difficult because of their small amount and small grain size. A separation of pure white micas was not possible. Parts of the sample were solved in acetic acid. The residuum was treated with hydrochloric acid for ca. 30 min. From this residuum, three samples were prepared: (1) bulk residuum, sieve fraction 63–125 μm, (2) bulk residuum <63 μm, and (3) residuum of sieve fraction 63–125 μm, enriched in white mica. The Rb-Sr data of the different fractions are plotted in Fig. 14 in addition to the Rb-Sr whole-rock data. A well-defined isochrone (MSWD <2.5) is not observed. This indicates initial Sr inhomogeneity of the sample. Uncertainties due to the leaching procedure are not probable as the acids used for leaching do not affect white mica. Nevertheless, the resulting age of 19.1 ±2.5 Ma (Fig. 14) should be considered as a value that is geologically significant.
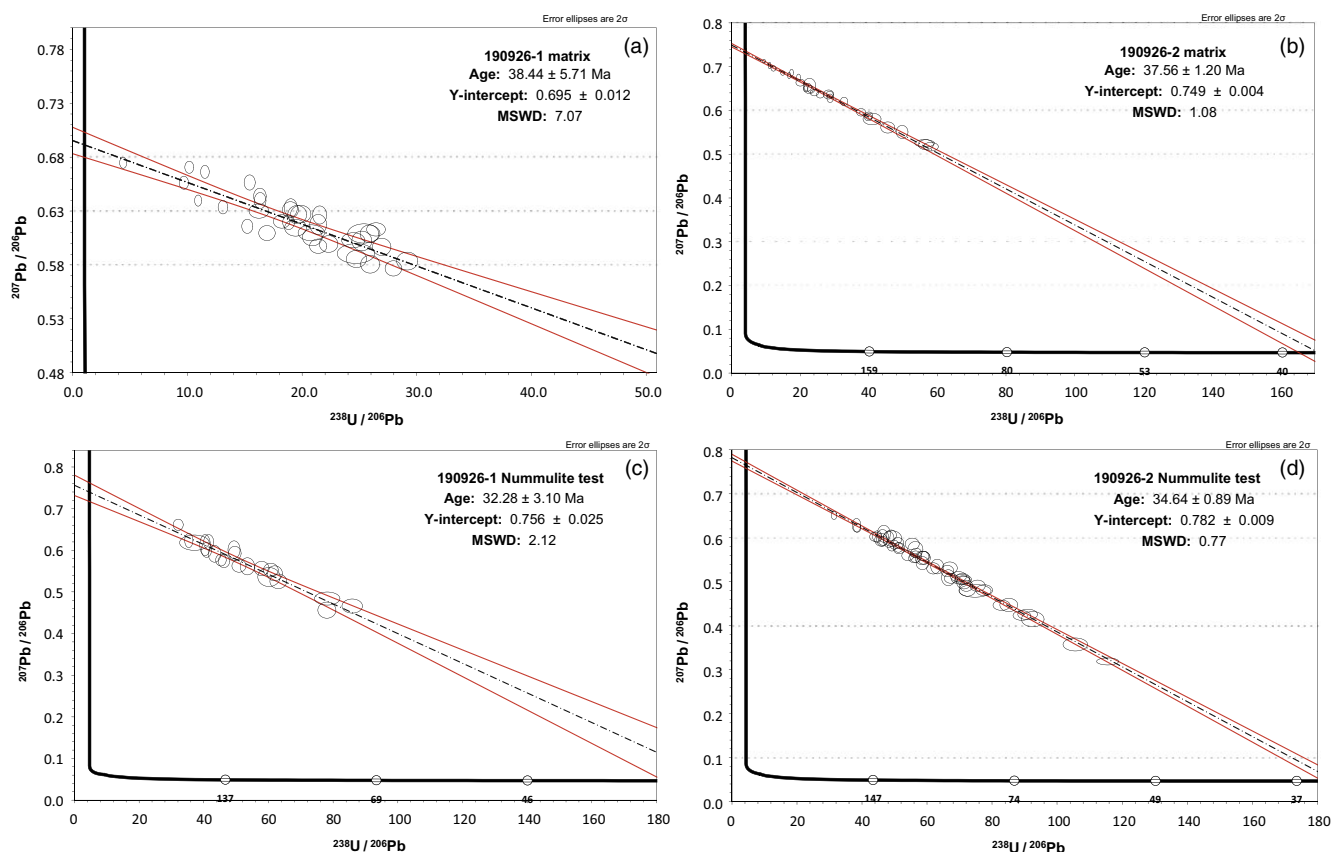
Figure 8. (Colour online) U-Pb data of matrix calcite (a, b) and of Nummulite test (c, d) of Nummulite-bearing (meta)limestone plotted in Tera-Wasserburg diagrams showing $^{207}Pb/^{206}Pb$ versus $^{238}U/^{206}Pb$. Data points are indicated as 2σ error ellipses. Sample numbers are indicated (see also Fig. 7).

5. Discussion

5.a. Deposition and diagenesis of Nummulite-bearing limestone olistolith

The dark *Nummulite*-bearing (meta)limestone exposed at Damnoni Bay is characteristic for the uppermost and youngest limy sequence of the TPU carbonate platform. In the Artemision Mountains of central Greece, similar thick-bedded dark *Nummulite*-bearing limestones are resting on top of rudist-bearing Upper Cretaceous limestones and are overlain by TPU flysch (Renz, 1913). This sequence is compatible with the fact that the TPU wildflysch of the Damnoni area includes olistoliths of both *Nummulite*- and rudist-bearing (meta)limestones. The age of the platform (meta)carbonates of the TPU exposed in the Sellia area should range from the Paleocene to the Priabonian (Karakitsios, 1982). Taking also data from the western Peloponnesus into account, the age of the subsequent Tripolitza flysch ranges from the early Priabonian to the late Oligocene/early Miocene (Fig. 15; Richter, 1976; Karakitsios, 1982; Fytrolakis & Antoniou, 1998).

The presence of *Pellatispira madaraszi* in the *Nummulite*-bearing (meta)limestone suggests a latest Bartonian to late Priabonian age (Özcan *et al.* 2019), which is in line with the age range mentioned above. Moreover, the U-Pb calcite ages of the fine-grained dark matrix (38.4 ±5.7 Ma and 37.6 ±1.2 Ma) should reflect the age of deposition at the Bartonian/Priabonian boundary (Fig. 15), which corresponds to a major faunal turnover in the Tethyan shallow marine ecosystems. Some new foraminiferal taxa, such as Heterostegina, appear for the first time, while major groups of large Nummulites and alveolinids disappear during Bartonian

and early Priabonian (Özcan *et al.* 2016a, 2016b). The large uncertainty of one of the above listed U-Pb matrix ages is probably related to the mixing of calcite crystals of different generations.

The younger U-Pb calcite ages (32.3 ±3.1 Ma and 34.6 ±0.9 Ma) obtained from fibres of the *Nummulite* tests reflect replacement of fibre calcite during late Priabonian/early Rupelian diagenesis (Fig. 15), which is in line with our trace element geochemical data. The chemical composition of the calcite fibres of the Nummulite test is not compatible with that of original fibres and thus must have changed during diagenesis. Against this background, the presence of the fibres as largely intact single crystals (as indicated by EBSD data, Fig. 6) is surprising and needs further investigations.

The period between the sedimentation of the dark (meta) limestone (*Nummulite* origin) and the change in composition of the *Nummulite* test was ca. 4 m.y. (Fig. 15). The replacement of the Nummulite calcite occurred at the Eocene/Oligocene boundary after the deposition of the first TPU flysch. This replacement should belong to a second phase of diagenesis. A first phase of diagenesis must have led to the consolidation of the dark (meta) limestone, while it was part of the carbonate platform. This first phase of diagenesis and consolidation was required for its removal and deposition as a large olistolith within the Tripolitza wildflysch.

The dark colour of the *Nummulite*-bearing (meta)limestone results from a relatively large amount of organic material, which indicates deposition under euxinic conditions. Such euxinic depositional environments occur when biological, physiographical or tectonic influences cause isolation of parts of the sea in which free access to the open ocean is restricted and varying degrees of stagnation of the bottom waters ensues (Krumbein & Sloss, 1963).
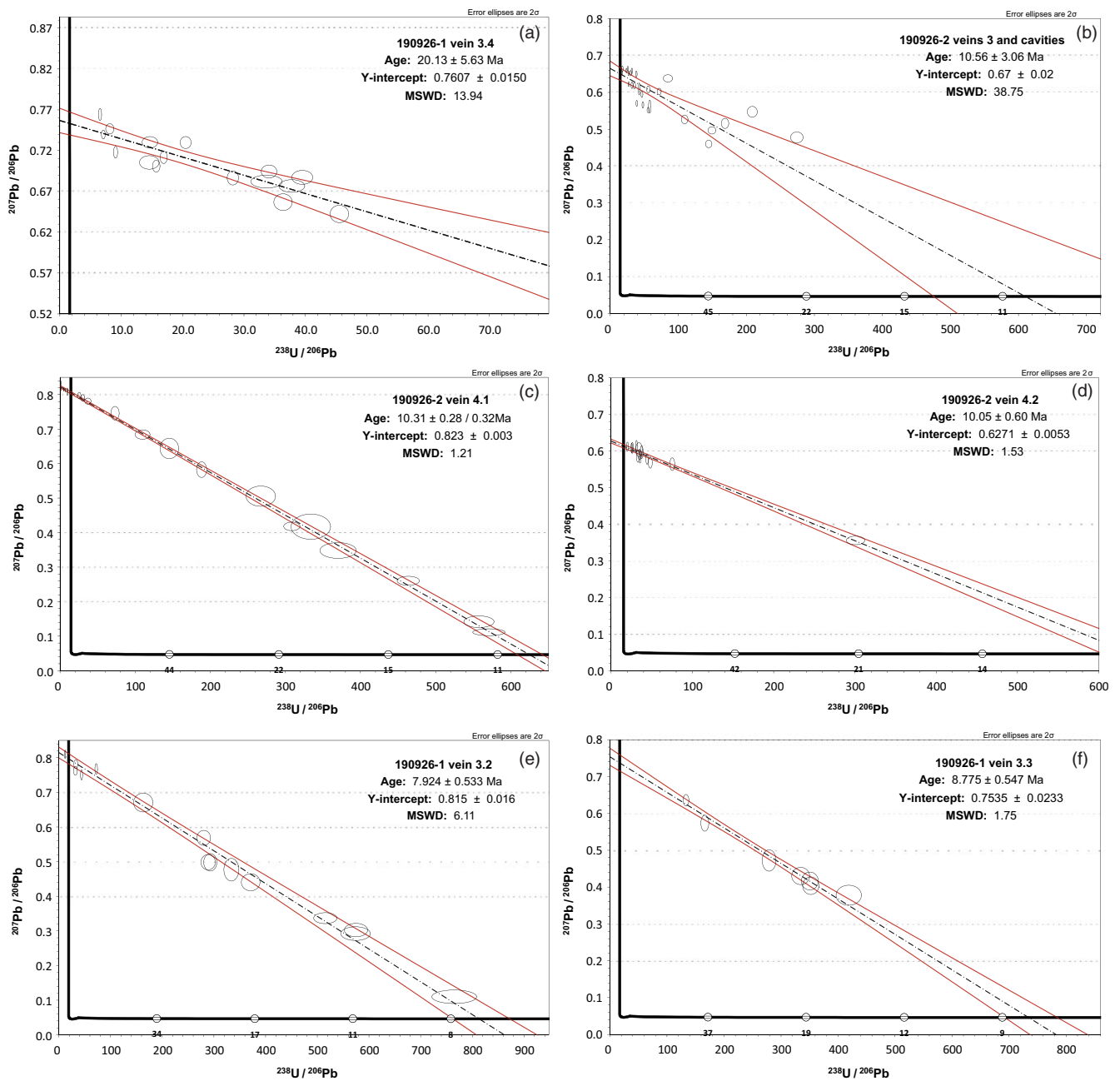
Figure 9. (Colour online) U–Pb data of calcite formed in veins and cavities of Nummulite-bearing (meta)limestone plotted in Tera-Wasserburg diagrams showing $^{207}Pb/^{206}Pb$ versus $^{238}U/^{206}Pb$ ratios. Data points are indicated as 2σ error ellipses. Sample locations and number of veins are indicated (see also Fig. 7).

Commonly euxinic bodies of water have an oxic, highly productive, thin surface layer, and have anoxic, sulfidic bottom water. Under these conditions, sediments are deposited in an anaerobic-reducing environment and are characterized by high organic content, presence of hydrogen sulfide and lack of a bottom fauna (Pettijohn, 1957). Uranium is a redox-sensitive element, which exhibits conservative behaviour in oxygenated water and exists in the dissolved oxycation ($UO_2{}^{2+}$) form but is reduced and becomes insoluble under anoxic conditions (Dang *et al.* 2018, and references therein). In the present case of the dark (meta)limestone, U was fixed during its deposition under euxinic conditions. This U is prone for U–Pb dating of the deposition of the

sediment using the calcite of the matrix. The presence of benthic foraminifera reveals that the boundary between oxidized and anoxic conditions was situated within the soft limy sediment. In the deeper anoxic parts, U became insoluble and was fixed. This fixed U could be dissolved after the conditions within the sediment had changed from anoxic to oxidized. Such a change should have occurred not only during the second phase of diagenesis (after the deposition of the wildflysch) but also during the different phases of vein formation. During each of these events, U that was initially fixed in the limy sediment could be removed via fluid phase replacing Ca during subsequent secondary calcite precipitation.
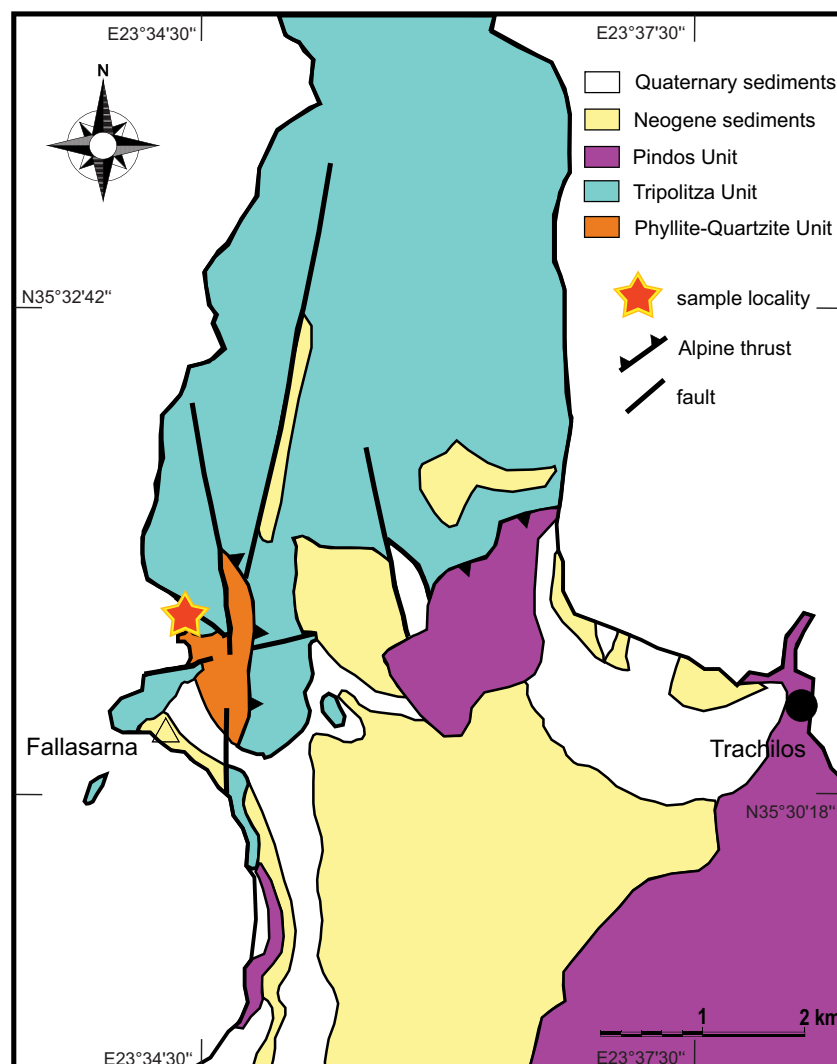
Figure 10. (Colour online) Geological map of study area north of Falasarna in NW Crete (after IGME).

5.b. Early Miocene subduction/collision of the Tripolitza Unit

As metamorphic index minerals are largely lacking in the carbonaceous lithology of the TPU, the temperature and pressure related to metamorphism are only poorly constrained. Nevertheless, there is a clear decrease in metamorphic temperature from the basal to the upper parts of the TPU. Average temperatures calculated from deconvoluted Raman spectra of carbonaceous material (CM) range from 286 to 351 °C (Klein *et al.* 2012). As CM is unlikely to change during retrogression of the host rock, these values can be regarded as minimum peak temperatures. The samples investigated in the present study reflect the minimum and the maximum values listed above.

The dark *Nummulite*-bearing (meta)limestone shows the lowest grade of metamorphism. It belongs to the youngest beds of the TPU carbonates and underwent deformation and metamorphism after being embedded as olistolith within the Tripolitza wildflysch. The Tripolitza flysch shows IC values at the diagenesis/anchizone transition (Klein *et al.* 2012) corresponding to $T = 240 \pm 15$ °C (Mullis *et al.* 2017). This low temperature is compatible with the entirely brittle deformation of the black (meta)limestone and with the type 1 twins found in calcite of all generations of veins. Type 1 twins result from deformation at $T < 200$ °C (Burkhard, 1993).

The mylonitic Tripolitza marble exposed north of Falasarna shows the highest grade of metamorphism of the TPU. The IC values in this area reflect epizonal conditions (Klein *et al.* 2012) corresponding to $T > 280$ °C (Ferreiro Mählmann, 2001). The growth of phengitic white mica and the calcite deformation microfabrics in the top-to-the WNW shear zone, which indicate recrystallization by subgrain rotation, suggest $T = $ ca. 310 °C (Fig. 13). Based on the Si content of the white mica, this temperature should be related to a minimum pressure of 0.3 GPa, which indicates a relatively low geothermal gradient most likely associated with slow subduction and/or collision (Fig. 13).

As the white mica of the Falasarna shear zone developed below the closure temperature of the Rb-Sr isotopic system of white mica, which is > 500 °C (e.g. Freeman *et al.* 1997; Glodny *et al.* 2008), the Rb-Sr age of the white mica (19.1 ± 2.5 Ma) should reflect the age of metamorphism of the TPU. Moreover, as the white mica grew syn-kinematically during ductile top-to-the WNW shearing, the Rb-Sr age should also date the shearing event.

It is difficult to determine the age of metamorphism of the anchimetamorphic TPU rocks deformed under brittle conditions. In the case of the dark *Nummulite*-bearing (meta)limestone, the oldest generation of calcite veins (vein I) should have formed during the peak of metamorphism as is indicated by its U-Pb age of
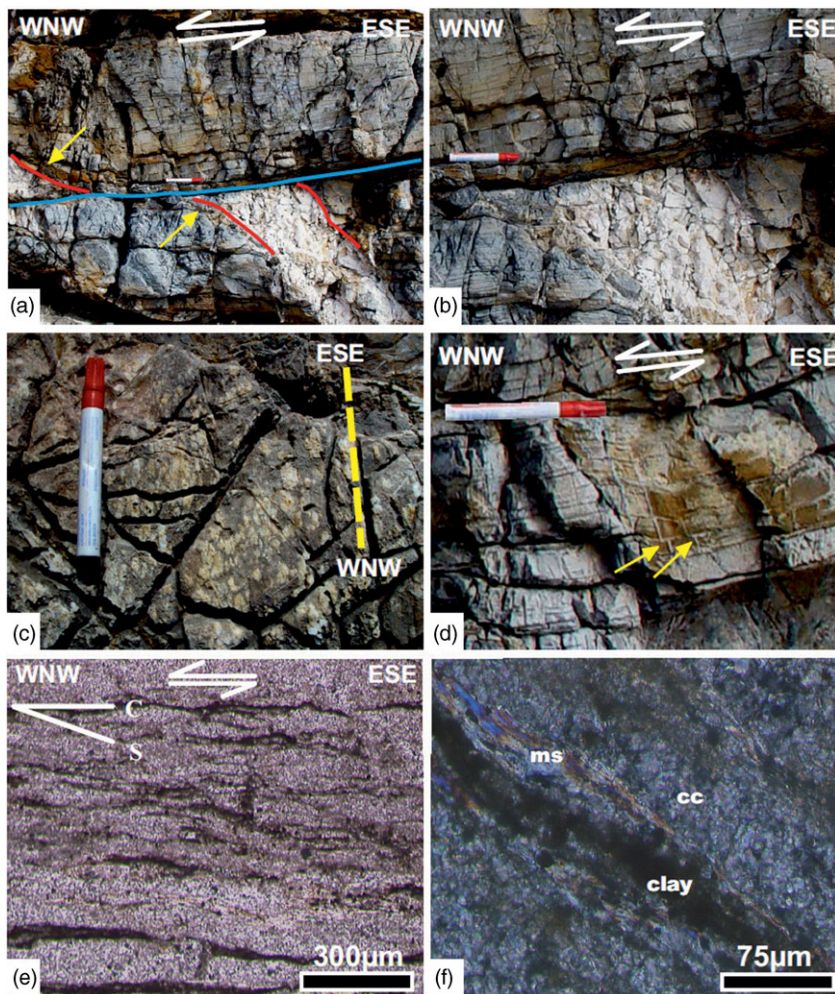
Figure 11. (Colour online) Ductile shear zone in Tripolitza marble exposed north of Falasarna in NW Crete (sample 020414/7-2). (a) Mylonitic foliation of shear zone largely subparallel to bedding (XZ-section); drag of sheared calcite vein (see yellow arrows) indicates top-to-the WNW shearing. (b) Detail of (a) showing the contact between vein and marble; sample with white mica shown in (e, f) was collected from the brownish foliated mylonite along the contact; (c) Mylonitic shear plane displaying WNW-ESE trending stretching lineation portrayed by elongated light calcite fragments. (d) Displacement of calcite veins along the mylonitic foliation (yellow arrows) indicates top-to-the WNW sense of shar. (e) Microphotograph (XZ-section) of calcite mylonite. Due to shearing, the dark stylolitic seams were changed into an SC fabric, which indicates top-to-the WNW sense of shear. (f) Synkinematic white mica (ms) besides clay minerals aligned subparallel to the mylonitic foliation of the shear zone. Matrix consists of recrystallized calcite (cc).

20 ±6 Ma. Although this age has a large uncertainty and MSWD, its mean value is compatible with the Rb-Sr age of white mica listed above (Fig. 15). As these oldest veins are very thin, the large MSWD of the U-Pb age is probably related to mixed sampling of calcite crystals of different generations during ablation. The low number of these early veins, compared to that of the younger veins, is probably related to the difference in metamorphic grade during vein formation. The early veins were formed under peak metamorphic conditions, which in the case of the Tripolitza flysch and thus of the *Nummulite*-bearing (meta)limestone olistolith, imply T = ca. 240 °C. Although this temperature is much lower than that inferred for the deformation of the Falasarna shear zone, it is sufficient to induce ductile deformation in fine-grained limestone by solution-precipitation creep and GBS, whereas fracturing was reduced. The younger veins (ca. 8–10 Ma), on the other hand, formed at T <100° C and thus under fully brittle conditions (see below). As the deformation during the top-to-the WNW shearing was largely ductile, the related ESE-WNW directed shortening is hardly documented by the twinning strain in the TPU (Klein *et al.* 2012), which, however, is widespread in the non-metamorphic Pindos rocks.

Top-to-the WNW thrusting of the TPU is compatible with the west-vergent folding of the Pindos Unit, which is well documented, for example, in the Cretaceous limestone-chert sequence along the southern coast of central Crete at Ag. Pavlos (e.g. Craddock *et al.* 2009: Fig. 3b, c). For this reason, it is assumed that the

WNW-directed shearing led to the emplacement of the Pindos nappe over the TPU. This thrusting event occurred during the early Miocene (ca. 19 Ma) and led to a pressure dominated metamorphic overprint of the Tripolitza rocks up to conditions of the epizone (T = ca. 320 °C at P_{min} = 0.3 GPa). Thrusting could have occurred in a subduction or collisional setting. The top-to-the west kinematics during collision of Pindos and TPU was active already during the Eocene when the Uppermost Unit was thrust on top of the Pindos Unit (Zulauf *et al.* in prep.).

5.c. Late Miocene emplacement of the Tripolitza nappe

The U-Pb ages obtained from the younger calcite veins can be separated into two generations both with a late Miocene (Tortonian) age. The older generation developed at ca. 10–11 Ma, which are slightly younger than U-Pb calcite ages reported from the nappe contact between TPU/Pindos Unit and the lower nappes (12–13 Ma, Ring *et al.* 2022). The younger generation was formed between 7 and 9 Ma (Fig. 15). Low-temperature geochronological data suggest that the opening of these veins should have occurred at T <120°C. Apatite fission-track ages and U-He zircon data yielded cooling below ca. 120 °C at 15–17 Ma (Rahl *et al.* 2005). These data are consistent with an apatite fission-track age of metatuffite (18 ±3 Ma, Thomson *et al.* 1999), which is intercalated in Tripolitza (meta)limestones. A similar apatite fission-track age (18 ±6 Ma) yielded a quartzite collected 500 m north of the black
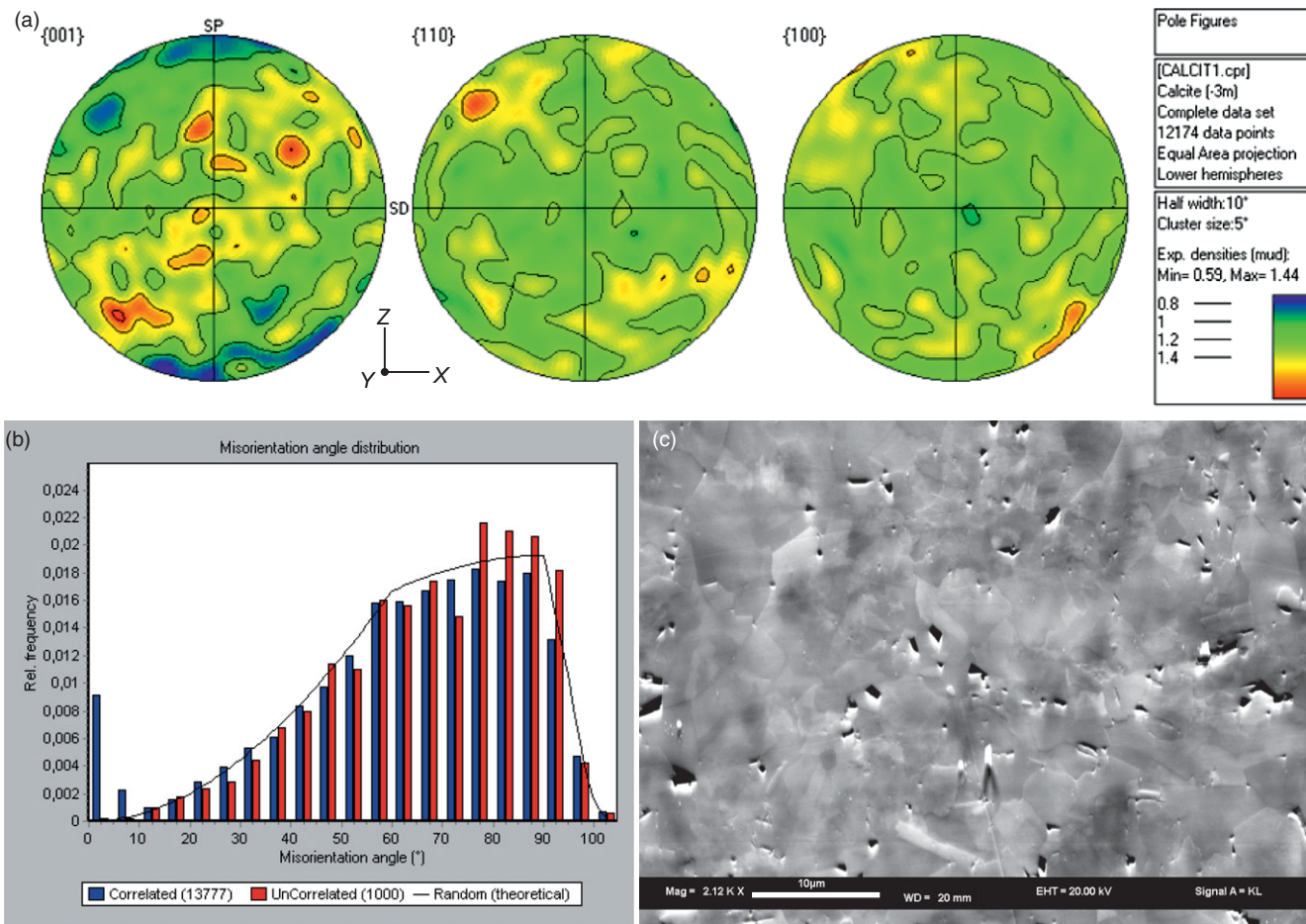
Figure 12. (Colour online) Microstructure and EBSD data of calcite of mylonitic shear zone (Falasarna, sample 020414/7-2). (a) Distribution of crystallographic axes of calcite shown in equal-area upper-hemisphere projection. Asymmetry of texture suggests a dextral sense of shear, which means top-top-the WNW in the field. (b) Misorientation data of calcite mylonite. (c) Scanning Electron Microscopy image of deformed calcite of mylonite (sample section: width 52 μm, height 39 μm, scale 10 μm). For further explanation, see text.
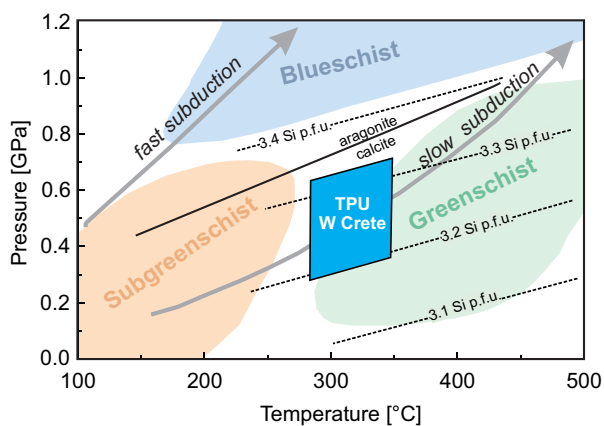

Figure 13. (Colour online) Pressure-temperature data of Tripolitza rocks exposed north of Falasarna. Temperature based on illite crystallinity and deformation microfabrics of calcite. Minimum pressure based on Si content of white mica. Si values of white mica, after Massonne and Schreyer (1987).
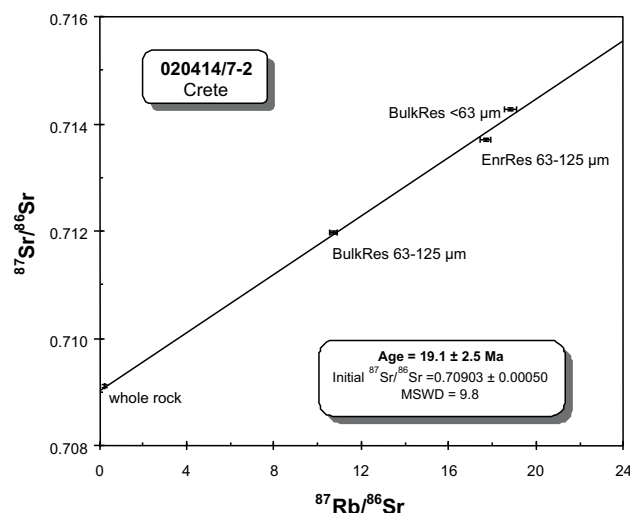

Figure 14. (Colour online) Rb-Sr data of white mica separated from ductile shear zone in Tripolitza marble N of Falasarna (sample 020414/7-2). Different size fractions in addition to whole-rock data are plotted in the isochrone diagram.

Nummulite-bearing (meta)limestone olistolith, and an even younger age of 13 ±4 Ma was obtained from a sandstone (Fig. 2, Thomson *et al.* 1999). However, the quartzite and the sandstone have been attributed to the Uppermost Unit by Thomson *et al.* (1999), although the fission-track ages in the Uppermost Unit are much higher (>30 Ma) and

sandstones have yet no been described from this unit. According to map Sellia (Karakitsios, 1982) and to our new mapping results of this area, both rocks belong to the Tripolitza flysch, which is compatible with their young fission-track ages.
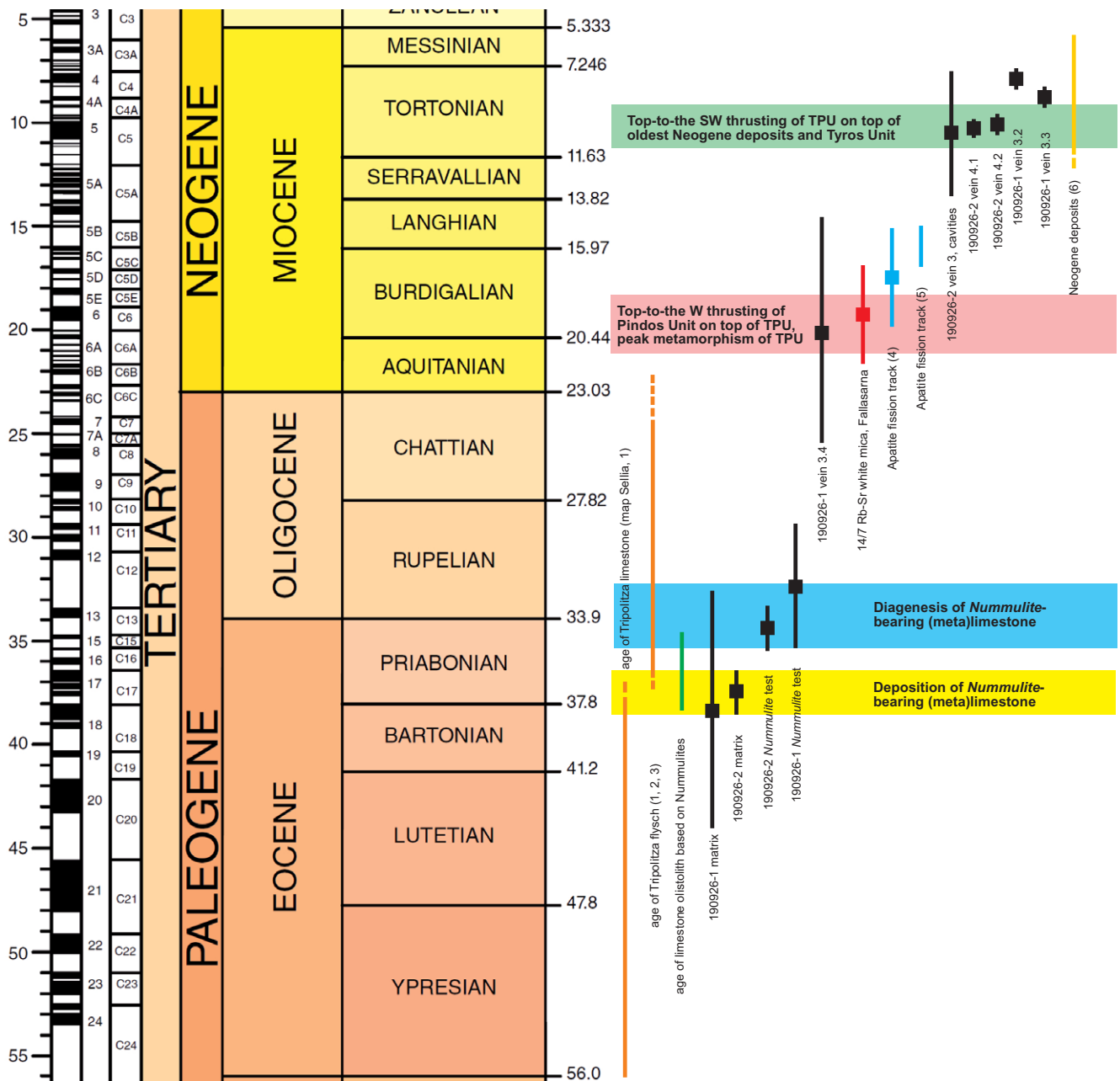
Figure 15. (Colour online) U-Pb calcite ages (black bars, this study) obtained from Nummulite test, matrix and veins of black Nummulite-bearing (meta)limestone olistolith, Rb-Sr age of synkinematic white mica (red bar, this study), and biostratigraphic age range of Nummulite limestone (green bar, this study), plotted besides age of Tripolitza (meta) carbonates and flysch (orange bars), fission-track ages of apatite (blue bars) and age of Neogene deposits (yellow bar). TPU = Tripolitza Unit. Reference keys: 1: Karakitsios, 1982; 2: Richter, 1976; 3: Fytrolakis and Antoniou, 1998; 4: Thomson *et al.* 1999; 5: Rahl *et al.* 2005; 6: Postma and Drinia, 1993.

The brittle deformation between 10 and 7 Ma at $T < 120$ °C, documented in the dark *Nummulite*-bearing (meta)limestone, should be related to the emplacement of the Tripolitza nappe on top of the lower Units. This conclusion is in line with a Tortonian to late Miocene age of thrusting of the TPU exposed on the Peloponnesus (Kowalczyk *et al.* 1977) and with top-to-the S thrusting of TPU rocks over Neogene conglomerates in eastern Crete (Kokkalas and Doutsos, 2001; Klein *et al.* 2012). Sedimentation of the Neogene deposits should have started between 15 and 10 Ma (Kopp & Richter, 1983; Fortuin & Peters, 1984; Postma & Drinia, 1993). The oldest robust ages of these deposits are ca. 11 Ma (Fassoulas, 2001; Ring *et al.* 2001; van Hinsbergen & Meulenkamp, 2006; Zachariasse *et al.* 2011). As the

components of these early Neogene sediments are derived only from the Upper nappes (Zachariasse *et al.* 2011), the lower Units (Plattenkalk, Phyllite-Quartzite s.str., Pre-Alpine Basement, and Tyros Unit) were below sea level during their deposition and probably also during the emplacement of the Tripolitza nappe. The cooling history of the lower nappes is well constrained. (1) K-Ar and ^{39}Ar-^{40}Ar ages of white mica obtained from phyllites of the Phyllite-Quartzite Unit s.str. of central and western Crete range from 24 to 19 Ma regarded as the time of HP-LT metamorphism (Seidel *et al.* 1982; Jolivet *et al.* 1996; Ring *et al.* 2022). (2) Fission-track ages of zircon yielded an arithmetic mean sample age at 18.6 ±1.9 Ma suggesting cooling below ca. 270 °C at this time (Thomson *et al.* 1998). (3) Zircon (U-Th)/He (ZHe) data, obtained

from rocks of the Tyros Unit of eastern Crete, suggest cooling <ca. 200 °C at 15 ±1 Ma (Grasemann *et al.* 2019). (4) Fission-track dating of apatite yielded an arithmetic mean sample age at 15.0 ±1.7 Ma (Thomson *et al.* 1998) and ages ranging from 9 to 12 Ma, Rahl *et al.* 2005). Thus, the TPU rocks reached the upper brittle structural level ($T <$ ca. 100 °C) earlier than, or coeval with, the deeper nappes.

Tripolitza samples from Falasarna area show slightly inclined shortening along a NE-SW trending axis resulting from layer-parallel shortening during SW-vergent recumbent folding, which postdates the ductile top-to-the WNW movements (Klein *et al.* 2012). The same holds for the Tripolitza flysch and the Pindos limestones. These rocks underwent subhorizontal NE-SW layer-parallel shortening, which is consistent with SW-vergent recumbent folding in the Platanos area (Klein *et al.* 2012). It is possible that after the peak of metamorphism was attained, the shortening direction in the TPU rotated continuously anticlockwise (with respect to the present coordinate system) until the N-S direction was reached. The structural data collected at the contact TPU/PQU s.l. are compatible with N-S contraction and consistently indicate southward directed movement of the TPU (Kokkalas and Doutsos, 2001; Klein *et al.* 2012, Kneuker *et al.* 2015; Ring & Yngwe, 2018). Kinematic data from the violet slates of the Tyros Unit in eastern Crete near the contact to the TPU suggest top-to-the N kinematics (Grasemann *et al.* 2019). However, as similar top-to-the N movements have been documented from rocks of the Phyllite-Quarzite Unit s.str. of eastern Crete, which partly reactivate pre-existing top-to-the S shear zones (Zulauf *et al.* 2002), and from the contact between the Phyllite-Quarzite s.str. and the Talea-Ori Unit (Seybold *et al.* 2018), these movements should be related to the exhumation of the deeper nappes as suggested by Jolivet *et al.* (1996).

The available low-temperature geochronological data suggest that the emplacement of the TPU (including the remains of its hanging nappes, Pindos and Uppermost Unit) did not cause heating of the deeper nappes to $T >100$°C. This conclusion is in line with a thickness of only 270 m for a stratigraphically complete section of the TPU carbonate platform in central Crete (Zambetakis-Lekkas *et al.* 1998). The nappe emplacement of the TPU was coeval with the development of the curvature of the Hellenic arc at ca. 10 Ma (Marsellos *et al.* 2010, Ring & Yngwe, 2018).

Based on the records of the Neogene sediments, the late Neogene tectonic evolution is characterized by normal faulting and oblique sinistral strike-slip, the latter occurring mainly in eastern Crete (ten Veen & Meijer 1998; ten Veen & Postma 1999; Kokkalas and Doutsos, 2001). Furthermore, younger block rotations affected Crete and caused differences up to several tens of degrees between the orientations of fault-bound blocks (Duermeijer *et al.* 1998).

The main principal shortening direction (ϵ_1) in the TPU, based on the calcite twinning strain, is trending N-S. One sub-maximum is vertical and a further one is directed NW-SE (Klein *et al.* 2012: Fig. 4b). Evidence for E-W shortening, which is well recorded in the Pindos rocks, is lacking in the TPU. The lack of evidence of E-W shortening strain in the TPU, portrayed by twinning in calcite, is related to the rheological condition during this event. E-W shortening occurred at ca. 19 Ma when the TPU rocks underwent peak metamorphism. Under these conditions (ca. 240–ca. 320 °C), the rocks of the TPU were deformed by solution-precipitation creep, subgrain rotation recrystallization and GBS, whereas vein formation and twinning of calcite were less relevant. The Pindos Unit, on the other hand, was situated at upper structural levels, where brittle deformation and twinning of calcite were dominant during the E-W shortening event.

The SW-vergent folding of the TPU in the Falasarna area is coeval with top-to-the S thrusting in eastern Crete. This deviation in shortening direction is also documented by the main stretching lineation in the Phyllite-Quarzite Unit s.l., which is trending NNE-SSW in western Crete but NNW-SSE in eastern Crete. This deviation is related to the late Miocene formation of the Hellenic arc. The youngest U-Pb calcite ages obtained from veins of the dark Nummulite limestone (7–9 Ma) could reflect crustal extension.

6. Conclusions

- Dark limestone, which is rich in organic material, is particularly prone for U-Pb calcite dating because U was fixed during its deposition under euxinic conditions. The integration of paleontological records with U-Pb calcite ages obtained from the limy matrix, foraminifers and tectonic veins of such black limestones allows constraining their complete development from sedimentation via diagenesis and burial to exhumation.
- The Upper Nappes of Crete have been stacked together by thin-skinned E-W shortening. Evidence for E-W shortening is poorly preserved in the TPU, where faults and folds are typically absent or obscured by karst. The early Miocene (19 ±2.5 Ma) top-to-the WSW shearing in the Falasarna outcrop is therefore of special importance.
- The emplacement of the TPU on top of late Miocene sediments and the lower nappes occurred during Tortonian (10–11 Ma) southward thrusting under brittle conditions. The related N-S shortening is well documented by calcite twinning strain.
- The variation in metamorphic degree within the TPU rocks cannot be explained solely by the TPU thickness but is also related to different depths during subduction/collision.
- The pseudomorphic replacement of single-crystal test fibres of Nummulites during late Priabonian/early Rupelian (ca. 35 Ma) diagenesis is an unexpected result and requires additional investigations.
- The upper and lower nappes of Crete differ significantly in the direction of tectonic shortening. Reconstructions of the Alpine geodynamic evolution in the Eastern Mediterranean should take into account the Miocene anticlockwise 90° rotation of the shortening direction as recorded in the TPU rocks.

References

Bestmann M and Prior DJ (2003) Intragranular dynamic recrystallization in naturally deformed calcite marble: diffusion accommodated grain boundary

sliding as a result of subgrain rotation recrystallization. *Journal of Structural Geology* 25, 1597–603.

Boiteau R, Greaves M and Elderfield H (2012) Authigenic uranium in foraminiferal coatings: a proxy for ocean redox chemistry. *Paleoceanography* 27, PA3227, doi: 10.1029/2012PA002335

Bonneau M (1984) Correlation of the Hellenide nappes in the south-east Aegean and their tectonic reconstruction, in: Robertson, A.H.F. and Dixon, J.E. The Geological Evolution of the Eastern Mediterranean. *Geological Society of London, Special Publication* 17, 517–27.

Bonneau M and Karakitsios V (1979) Lower (Upper Triassic) Horizons of the Tripolitza Nappe in Crete (Greece) and their relationship with the phyllite nappe—problems of stratigraphy, tectonics and metamorphism. *Comptes Rendus de l'Académie des Sciences, Série D* 28, 15–8.

BouDagher-Fadel MK (2008) Evolution and geological significance of larger Benthic Foraminifera. *Developments in Palaeontology and Stratigraphy* Elsevier, Amsterdam, 21, 540.

Burisch M, Gerdes A, Walter BF, Neumann U, Fettel M and Markl G (2017) Methane and the origin of five-element veins: mineralogy, age, fluid inclusion chemistry and ore forming processes in the Odenwald, SW Germany. *Ore Geology Reviews* 81, 42–61.

Burkhard M (1993) Calcite twins, their geometry, appearance and significance as stress-strain markers and indicators of tectonic regime: a review. *Journal of Structural Geology* 15, 351–68.

Chatzaras V, Xypolias P and Doutsos T (2006) Exhumation of high-pressure rocks under continuous compression: a working hypothesis for the southern Hellenides (central Crete, Greece). *Geological Magazine* 143, 859–76. doi: 10.1017/S0016756806002585.

Coogan LA, Parrish RR and Roberts NM (2016) Early hydrothermal carbon uptake by the upper oceanic crust: Insight from in situ U-Pb dating. *Geology* 44, 147–50. doi: 10.1130/G37212.1.

Cotton LJ, Evans D and Beavington-Penney SJ (2020) The high-magnesium calcite origin of nummulitid foraminifera and implications for the identification of calcite diagenesis. *Palaios* 35, 421–31. doi: 10.2110/palo.2020.029.

Cotton LJ and Pearson PN (2011) Extinction of larger benthic foraminifera at the Eocene/Oligocene boundary. *Palaeogeography, Palaeoclimatology, Palaeoecology* 311, 281–96. doi: 10.1016/j.palaeo.2011.09.008.

Craddock JP, Klein T, Kowalczyk G and Zulauf G (2009) Calcite twinning strains in Alpine orogen flysch: implications for thrustnappe mechanics and the geodynamics of Crete. *Lithosphere* 1, 174–91.

Creutzburg N and Seidel E (1975) Zum Stand der Geologie des Präneogens auf Kreta. *Neues Jahrbuch für Geologie und Paläontologie, Abhandlungen* 149, 363–83.

Dang DH, Evans RD, Wang W, Omanović D, El Houssainy A, Lenoble V, Mullot J-U, Mounier S and Garnier C (2018) Uranium isotope geochemistry in modern coastal sediments: insights from Toulon Bay, France. *Chemical Geology* 481, 133–45. doi: 10.1016/j.chemgeo.2018.01.032.

De Bresser JHP and Spiers CJ (1997) Strength characteristics of the r, f, and c slip systems in calcite. *Tectonophysics* 272, 1–23.

Duermeijer CE, Krijgsman W, Langereis CG and ten Veen JH (1998) Post-early Messinian counterclockwise rotations on Crete: implications for late Miocene to recent kinematics of the southern Hellenic arc. *Tectonophysics* 298, 177–89.

Dunham RJ (1962) Classification of carbonate rocks according to depositional texture. In *Classification of Carbonate Rocks* (ed WE Ham), 108–21. Tulsa: AAPG.

Evans D and Müller W (2018) Automated extraction of a five-year LA-ICP-MS trace element data set of ten common glass and carbonate reference materials: long-term data quality, optimisation and laser cell homogeneity. *Geostandards and Geoanalytical Research* 42, 159–88. doi: 10.1111/ggr.12204.

Evans D, Müller W, Oron S and Renema W (2013) Eocene seasonality and seawater alkaline earth reconstruction using shallow-dwelling large benthic foraminifera. *Earth and Planetary Science Letters* 381, 104–15. doi: 10.1016/j.epsl.2013.08.035.

Evans D, Sagoo N, Renema W, Cotton LJ, Müller W, Todd JA, Saraswati PK, Stassen P, Ziegler M, Pearson PN, Valdes PJ and Affek HP (2018) Eocene greenhouse climate revealed by coupled clumped isotope-Mg/Ca thermometry. *Proceedings of the National Academy of Sciences* 115, 1174–9. doi: 10.10 73/pnas.1714744115.

Fassoulas C (2001) The tectonic development of a Neogene basin at the leading edge of the active European margin: the Heraklion basin, Crete, Greece. *Journal of Geodynamics* 31, 49–70.

Fassoulas C, Kilias A and Mountrakis D (1994) Postnappe stacking extension and exhumation of high-pressure/low-temperature rocks in the island of Crete, Greece. *Tectonics* 13, 127–238.

Feldhoff AR, Theye T and Richter KD (1993) Coal rank versus illite crystallinity and estimated, p-T conditions: some problems concerning the Pindos, Triplolitza and Phyllite-Quartzite Series in Crete. *Bulletin of the Geolgical Society of Greece* 28, 603–15.

Feldhoff RA, Lücke A and Richter KD (1991) Über die Diagenese/ Metamorphosebedingungen der Pindos-und Tripolitza-Serie auf der Insel Kreta (Griechenland). *Zentralblatt für Geologie und Paläontologie Teil I* 1990, 1611–22.

Ferreiro Mählmann R (2001) Correlation of very low grade data to calibrate a thermal maturity model in a nappe tectonic setting, a case study from the Alps. *Tectonophysics* 334, 1–33.

Ferrill D Morris A, Evans M, Burkhard M, Groshong R and Onasch C (2004) Calcite twin morphology: a low-temperature deformation geothermometer. *Journal of Structural Geology* 26, 1521–9.

Fietzke J and Frische M (2016) Experimental evaluation of elemental behavior during LA-ICP-MS: influences of plasma conditions and limits of plasma robustness. *Journal of Analytical Atomic Spectrometry* 31, 234–44. doi: 10.1039/C5JA00253B.

Fortuin AR and Peters JM (1984) The Prina complex in eastern Crete and its relationship to possible Miocene strike-slip tectonics. *Journal of Structural Geology* 6, 459–76.

Freeman SR, Inger S, Butler RWH and Cliff RA (1997) Dating deformation using Rb–Sr in white mica: greenschist facies deformation ages from the Entrelor shear zone, Italian Alps. *Tectonics* 16, 57–76.

Fytrolakis N and Antoniou M (1998) Contribution to the knowledge of the Gavrovou subzone flysch formations, in the Messenia and in the area of the Klokova and Varasova. *Bulletin Geological Society of Greece* 32, 23–31.

Garbe-Schönberg D and Müller S (2014) Nano-particulate pressed powder tablets for LA-ICP-MS. *Journal of Analytical Atomic Spectrometry* 29, 990–1000.

Gerdes A and Zeh A (2009) Zircon formation versus zircon alteration—new insights from combined U–Pb and Lu–Hf in-situ LA-ICP-MS analyses, and consequences for the interpretation of Archean zircon from the Central Zone of the Limpopo Belt. *Chemical Geology* 261, 230–43.

Glodny J, Kühn A and Austrheim H (2008) Diffusion versus recrystallization processes in Rb–Sr geochronology: isotopic relics in eclogite facies rocks, Western Gneiss Region, Norway. *Geochimica et Cosmochimica Acta* 72, 506–25.

Godeau N, Deschamps P, Guihou A, Leonide P, Tendil A, Gerdes A, et al. (2018) U-Pb dating of calcite cement and diagenetic history in microporous carbonate reservoirs: case of the Urgonian Limestone, France. *Geology* 46, 247–50.

Grasemann B, Schneider DA and Rogowitz A (2019) Back to normal: direct evidence of the Cretan Detachment as a north-directed normal fault during the miocene. *Tectonics* 38, 3052–69. doi: 10.1029/2019TC005582.

Hansman RJ, Albert R, Gerdes A and Ring U (2018) Absolute ages of multiple generations of brittle structures by U-Pb dating of calcite. *Geology* 46, 207–10.

Haude G (1989). *eologie der Phyllit-Einheit im Gebiet um Palekastro (Nordost-Kreta, Griechenland)*. Published PhD thesis, 131 pp., Technical University of Munich, Germany.

Hauzer H, Evans D, Müller W, Rosenthal Y and Erez J (2018) Calibration of Na partitioning in the calcitic foraminifer Operculina ammonoides under variable Ca concentration: toward reconstructing past seawater composition. *Earth and Planetary Science Letters* 497, 80–91.

Israelson C, Halliday AN and Buchardt B (1996) U-Pb dating of calcite concretions from Cambrian black shales and the Phanerozoic time scale. *Earth and Planetary Science Letters* 141, 153–9.

Jahn B, Bertrand-Sarfati J, Morin N and Mace J (1990) Direct dating of stromatolitic carbonates from the Schmidtsdrif Formation (Transvaal

Dolomite), South Africa, with implications on the age of the Ventersdorp Supergroup. *Geology* **18**, 1211–4.

Jahn B-M and Cuvellier H (1994) Pb-Pb and U-Pb geochronology of carbonate rocks: an assessment. *Chemical Geology* **115**, 125–51.

Jochum KP, Stoll B, Herwig K, Willbold M, Hofmann AW, Amini M, et al. (2006) MPI-DING reference glasses for in situ microanalysis: new reference values for element concentrations and isotope ratios. *Geochemistry, Geophysics, Geosystems* **7**, 1–44. doi: 10.1029/2005GC001060.

Jochum KP, Weis U, Stoll B, Kuzmin D, Yang Q, Raczek I, Jacob DE, Stracke A, Birbaum K, Frick DA, Günther D and Enzweiler J (2011) Determination of Reference Values for NIST SRM 610–617 glasses following ISO guidelines. *Geostandards and Geoanalytical Research* **35**, 397–429. doi: 10.1111/j.1751-908X.2011.00120.x.

Jolivet L, Goffé B, Monié P, Truffert-Luxey C, Patriat M and Bonneau M (1996) Miocene detachment in Crete and exhumation P-T-t paths of high-pressure metamorphic rocks. *Tectonics* **15**, 1129–53.

Karakitsios V (1982) *Geological map of Greece. Sheet Sellia (Crete) 1:50.000.* I.G.M.E., Athens, https://www.eagme.gr/

Kelly SD, Newville MG, Cheng L, Kemner KM, Sutton SR, Fenter P, Sturchio NC and Spötl C (2003) Uranyl incorporation in natural calcite. *Environmental Science & Technology* **37**, 1284–7.

Kelly SD, Rasbury ET, Chattopadhyay S, Kropf AJ and Kemner KM (2006) Evidence of a stable Uranyl site in ancient organic-rich calcite. *Environmental Science & Technology* **40**, 2262–8.

Keul N, Langer G, De Nooijer LJ, Nehrke G, Reichart GJ and Bijma J (2013) Incorporation of uraniumin in benthic foraminiferal calcite reflects seawater carbonate ion concentration. *Geochemistry, Geophysics, Geosystems* **14**, 102–11.

Klein T, Craddock JP and Zulauf G (2012) Constraints on the geodynamical evolution of Crete: insights from illite crystallinity, Raman spectroscopy and calcite twinning above and below the "Cretan Detachment". *International Journal of Earth Sciences* **102**, 139–82. doi: 10.1007/s00531-012-0781-4.

Klein T, Reichhardt H, Klinger L, Grigull S, Wostal G and Zulauf G (2008) Reverse slip along the contact Phyllite-Quartzite Unit/Tripolitza unit in eastern Crete: implications for the geodynamic evolution of the External Hellenides. *New Results and Concepts on the Regional Geology of the Eastern Mediterranean* (eds Xypolias, P. & Zulauf, G.), *Zeitschrift der Deutschen Gesellschaft für Geowissenschaften* **159**, 375–98.

Klein T, Zulauf G, Craddock J and Glodny J (2006) Methodische Untersuchungen am Kreta-Detachment (Kreta, Griechenland): Anzeichen für eine alpidische Metamorphose der Hangendscholle, TSK 11. In *11. Symposium "Tektonik, Struktur- und Kristallingeologie" -Zusammenfassung der Tagungsbeiträge* (eds S Philipp, B Leiss, A Vollbrecht, D Tanner and A Gudmundsson), pp. 108–11. Universitätsverlag Göttingen, Göttingen, Germany, doi: 10.23689/FIDGEO-3.

Kneuker T, Dörr W, Petschick R and Zulauf G (2015) Upper crustal emplacement and deformation of granitoids inside the Uppermost Unit of the Cretan nappe stack: constraints from U–Pb zircon dating, microfabrics and paleostress analyses. *International Journal of Earth Sciences (Geol Rundsch)* **104**, 351–67. doi: 10.1007/s00531-014-1088-4.

Kokkalas S and Doutsos T (2001) Strain-dependent stress field and plate motions in the south-east Aegean region. *Journal of Geodynamics* **32**, 311–32.

Kowalczyk G, Richter D, Risch H and Winter KP (1977) Zur zeitlichen Einstufung der tektogenetischen Ereignisse auf dem Peloponnes (Griechenland). (The timing of the tectogenetic development of the Peloponnesus, Greece). *Neues Jahrbuch fuer Geologie und Palaeontologie, Monatshefte* **9**, 541–64.

Kopp K-O and Richter D (1983) Synorogenetische Schuttbildungen und die Eigenständigkeit der Phyllit-Gruppe auf Kreta. *Neues Jahrbuch für Geologie und Paläontologie, Abhandlungen* **165**, 228–53.

Krumbein WC and Sloss LL (1963) *Stratigraphy and Sedimentation*, 2nd edn. San Francisco: W.H. Freeman and Company, 660 pp.

Less G, Özcan E, Papazzoni CA and Stockar R (2008) The middle to late Eocene evolution of nummulitid foraminifer *Heterostegina* in the Western Tethys. *Acta Palaeontologica Polonica* **53**, 317–50.

Longerich HP, Jackson SE and Günther D (1996) Laser ablation inductively coupled plasma mass spectrometric transient signal data acquisition and analyte concentration calculation. *Journal of Analytical Atomic Spectrometry* **11**, 899–904.

Ludwig KR (1999) *User's Manual for Isoplot/Ex, version 2.10, a Geochronological Toolkit for Microsoft Excel.* Berkeley, CA: Berkeley Geochronology Center Special Publication.

Manutsoglu E, Mertmann D and Jacobshagen V (1993) Zur faziellen Entwicklung triassischer Gesteinsfolgen der Tripolitza-Plattform in Süd-Lakonien (Peloponnes/Griechenland). *Zeitschrift der Deutschen Geologischen Gesellschaft* **144**, 396–405.

Marsellos AE, Kidd WSF and Garver JI (2010) Extension and exhumation of the HP/LT rocks in the Hellenic fore-arc ridge. *American Journal of Science* **310**, 1–36.

Massonne H-J and Schreyer W (1987) Phengite geobarometry based on the limiting assemblage with K-feldspar, phlogopite and quartz. *Contributions to Mineralogy and Petrology* **96**, 212–24.

Massonne H-J and Szpurka Z (1997) Thermodynamic properties of White Micas on the basis of high-pressure experiments in the systems K2O-MgO-Al2O3-H2O and K2O-FeO-Al2O3-SiO2-H2O. *Lithos* **41**, 229–50. doi: 10.1016/S0024-4937(97)82014-2

Müller W, Shelley M, Miller P and Broude S (2009) Initial performance metrics of a new custom-designed ArF excimer LA-ICPMS system coupled to a two-volume laserablation cell. *Journal of Analytical Atomic Spectrometry* **24**, 209–14. doi: 10.103 9/B805995K.

Mullis J, Ferreiro-Mählmann R and Wolf M (2017) Fluid inclusion microthermometry to calibrate vitrinite reflectance (between 50 and 270 °C), illite Kübler-Index data and the diagenesis/anchizone boundary in the external part of the Central Alps. *Applied Clay Science* **143**, 307–19. doi: 10.1016/j.clay.2017.03.023.

Nuriel P, Weinberger R, Kylander-Clark ARC, Hacker BR and Craddock JP (2017) The onset of the Dead Sea transform based on calcite age-strain analyses. *Geology* **45**, 587.

Özcan E, Ali N, Hanif M, Hashmi SI, Khan A, et al. (2016a) New Priabonian Heterostegina from the Eastern Tethys (Sulaiman fold belt, West Pakistan): implications for the development of Eastern Tethyan heterostegines and their paleobiogeography. *Journal of Foraminiferal Research* **46**, 393–408.

Özcan E, Less G, Okay A, Báldi-Beke M, Kollányi K and Yilmaz İ (2010) Stratigraphy and larger foraminifera of the Eocene shallow marine and olistostromal units of the southern part of the Thrace Basin, NW Turkey. *Turkish Journal of Earth Sciences* **19**, 27–77.

Özcan E, Saraswati PK, Hanif M and Ali N (2016b) Orthophragminids with new axial thickening structures from the Bartonian of the Indian subcontinent. *Geologica Acta* **14**, 261–82.

Özcan E, Yücel AO, Erbay S, Less G, Kaygili S, Ali N and Hanif M (2019) Reticulate Nummulites (N. fabianii Linage) and age of the Pellatispira-Beds of the Drazinda formation, Sulaiman Range, Pakistan. *International Journal of Paleobiology and Paleontology* **2**, 000105.

Papanikolaou D and Vassilakis E (2010) Thrust faults and extensional detachment faults in Cretan tectono-stratigraphy: implications for Middle Miocene extension. *Tectonophysics* **488**, 233–47. doi: 10.1016/j.tecto.2009.06.024.

Papazzoni CA, Ćosović V, Briguglio A and Drobne K (2017) Towards a calibrated larger foraminifera biostratigraphic zonation: celebrating 18 years of the application of shallow benthic zones. *Palaios* **32**, 1–4.

Pettijohn FJ (1957) *Sedimentary Rocks*, 2nd Edn. New York: Harper and Brothers, 718 pp.

Postma G and Drinia H (1993) Architecture and sedimentary facies evolution of a marine, expanding outer-arc half-graben (Crete, late Miocene). *Basin Research* **5**, 103–24.

Purton LMA and Brasier MD (1999) Giant protist Nummulites and its Eocene environment: life span and habitat insights from $\delta^{18}O$ and $\delta^{13}C$ data from Nummulites and Venericardia, Hampshire basin, UK. *Geology* **27**, 711–4.

Rahl JM, Anderson KM, Brandon MT and Fassoulas C (2005) Raman spectroscopic carbonaceous material thermometry of low-grade metamorphic rocks: calibration and application to tectonic exhumation in Crete, Greece. *Earth and Planetary Science Letters* **240**, 339–54.

Raitzsch M, Kuhnert H, Hathorne EC, Groeneveld J and Bickert T (2011) U/Ca in benthic foraminifers: a proxy for the deep-sea carbonate saturation. *Geochemistry, Geophysics, Geosystems* **12**, 1–12.

Rasbury ET and Cole JM (2009) Directly dating geologic events: U-Pb dating of carbonates. *Reviews of Geophysics* **47**, 1–27.

Renz C (1913) Geologische Studien im Artemisiongebirge (Grenze von Arkadien und Argolis). In Beiträge zur Geologie von Hellas und der angrenzenden Gebiete (eds Renz, C. & Frech, F.). *Zentralblatt für Mineralogie, Geologie und Palaeontologie* **1913**, 338–46.

Renz C (1955) *Die vorneogene Stratigraphie der normalsedimentären Formationen Griechenlands*. Athens: Institute for Geology and Subsurface Research, 637pp.

Richards DA, Bottrell SH, Cliff RA, Strohle K and Rowe PJ (1998) U-Pb dating of a speleothem of Quaternary age. *Geochimica et Cosmochimica Acta* **62**, 3683–8.

Richter D (1976) Das Flysch-Stadium der Helleniden – Ein Überblick. *Zeitschrift der Deutschen Geologischen Gesellschaft* **127**, 467–83.

Ring U, Brachert T and Fassoulas C (2001) Middle Miocene graben development in Crete and its possible relation to large-scale detachment faults in the southern Aegean. *Terra Nova* **13**, 297–304.

Ring U, Fassoulas C, Uysal IT, Bolhar R, Tong K and Todd A (2022) Nappe imbrication within the Phyllite-Quartzite Unit of West Crete: Implications for sustained high-pressure metamorphism in the Hellenide subduction orogen, Greece. *Tectonics* **41**, e2022TC007430. doi: 10.1029/2022TC007430.

Rittner M and Müller W (2011) Dating Brittle deformation with the U-Pb method. *Geophysical Research Abstracts* **13**, EGU2011-13443; EGU General Assembly 2011.

Ring U and Gerdes A (2016) Kinematics of the Alpenrhein-Bodensee graben system in the Central Alps: Oligocene/Miocene transtension due to formation of the Western Alps arc. *Tectonics* **35**, 1367–91. doi: 10.1002/2015TC004085.

Ring U and Yngwe F (2018) "To Be, or Not to Be, That Is the Question"— The Cretan Extensional Detachment, Greece. *Tectonics* **37**, 3069–84. doi: 10.1029/2018TC005179.

Roberts NMW and Walker RJ (2016) U-Pb geochronology of calcite-mineralized faults: absolute timing of rift-related fault events on the NE Atlantic margin. *Geology* **44**, 531–53. doi: 10.1130/G37868.1.

Robertson AHF (2006) Sedimentary evidence from the south Mediterranean region (Sicily, Crete Peloponnese), used to test alternative tectonic models for the regional tectonic setting of Tethys during Late Palaeozoic-Early Mesozoic time. In *Tectonic development of the Eastern Mediterranean Region* (eds AHF Robertson and D Mountrakis), **260**, pp. 91–154. London, United Kingdom: Geological Society of London, Special Publications.

Robertson AHF (2012) Late Palaeozoic–Cenozoic tectonic development of Greece and Albania in the context of alternative reconstructions of Tethys in the Eastern Mediterranean region. *International Geology Review* **54**, 373–454.

Russell AD, Emerson S, Nelson BK, Erez J and Lea DW (1994) Uranium in foraminiferal calcite as a recorder of seawater uranium concentrations. *Geochimica et Cosmochimica Acta* **58**, 671–81.

Schaub H (1981) Nummulites et Assilines de la Téthys Paléogène. Taxonomie, phylogenèse et biostratigraphie. *Schweizerische Paläontologische Abhandlungen* **1981**, 104–106.

Schmidt N-H and Olesen NO (1989) Computer-aided determination of crystal-lattice orientation from electron-channeling patterns in the SEM. *Canadian Mineralogist* **27**, 15–22.

Seidel E, Kreuzer H and Harre W (1982) A late Oligocene/early Miocene high pressure belt in the external Hellenides. *Geologisches Jahrbuch* **E23**, 165–206.

Seidel E and Wachendorf H (1986) Die Südägäische Inselbrücke. In *Geologie von Griechenland* (ed V Jacobshagen), pp. 54–80. Berlin: Borntraeger.

Serra-Kiel J, Hottinger L, Caus E, Drobne K, Ferrandez F, Jauhri AK, *et al.* (1998) Larger foraminiferal biostratigraphy of the Tethyan Paleocene and Eocene. *Bulletin de la Société géologique de France* **169**, 281–99.

Seybold L, Trepmann CA and Janots E (2018) A ductile extensional shear zone at the contact area between HP-LT metamorphic units in the Talea Ori, central Crete, Greece: deformation during early stages of exhumation from peak metamorphic conditions. *International Journal of Earth Sciences* **108**, 213–27. doi: 10.1007/s00531-018-1650-6.

Smith PE, Brand U and Farquhar RM (1994) U-Pb systematics and alteration trends of Pennsylvanian-aged aragonite and calcite. *Geochimica et Cosmochimica Acta* **58**, 313–22.

Stampfli GM and Kozur H (2006) Europe from the Variscan to the Alpine cycles. In *European Lithosphere Dynamics* (eds DG Gee and RA Stephenson), **32**, pp. 57–82, Memoir, London, United Kingdom: Geological Society of London.

Sturchio NC, Antonio MR, Soderholm L, Sutton SR and Brannon JC (1998) Tetravalent uranium in calcite. *Science* **281**, 971–3.

ten Veen JH and Meijer PT (1998) Late Miocene to recent tectonic evolution of Crete (Greece): geological observations and model analysis. *Tectonophysics* **298**, 191–208.

ten Veen JH and Postma G (1999) Neogene tectonics and basin fill patterns in the Hellenic outer-arc (Crete, Greece). *Basin Research* **11**, 223–41.

Thomson SN, Stöckhert B and Brix MR (1998) Thermochronology of the high-pressure metamorphic rocks of Crete, Greece: implications for the speed of tectonic processes. *Geology* **26**, 259–62.

Thomson SN, Stöckhert B and Brix MR (1999) Miocene high-pressure metamorphic rocks of Crete, Greece: rapid exhumation by buoyant escape. *Geological Society of London, Special Publications* **154**, 87–107.

Thorbecke G (1976) Nachweis von Tripolitza-Flysch auf der Insel Kasos/Griechenland. *Zeitschrift der Deutschen Geologischen Gesellschaft* **127**, 125–31.

Tsaila-Monopolis S (1977) Micropaleontological and stratigraphical study of the Tripolitza (Gavrovo) Zone in the Peloponnesus. *Geol. Geophys. Res., Institute for Geology and Subsurface Research, Athens* **20**, 1–99.

van Hinsbergen DJJ and Meulenkamp JE (2006) Neogene supradetachment basin development on Crete (Greece) during exhumation of the South Aegean core complex. *Basin Research* **18**, 103–24. doi: 10.1111/j.1365-2117.2005.00282.x.

Weremeichik JM, Gabitov RI, Thien BMJ and Sadekov A (2017) The effect of growth rate on uranium partitioning between individual calcite crystals and fluid. *Chemical Geology* **450**, 145–53.

Wefer G and Berger W (1980) Stable isotopes in benthic foraminifera: seasonal variation in large tropical species. *Science* **209**, 803.

Xypolias P and Kokkalas S (2006) Heterogeneous ductile deformation along a mid-crustal extruding shear zone: an example from the External Hellenides (Greece). *Geological Society, London, Special Publications* **268**, 497–516. doi: 10.1144/GSL.SP.2006.268.01.23.

Zachariasse WJ, Van Hinsbergen DJJ and Fortuin AR (2011) Formation and fragmentation of a late Miocene supradetachment basin in central Crete: implications for exhumation mechanisms of high-pressure rocks in the Aegean forearc. *Basin Research* **23**, 678–701.

Zambetakis-Lekkas A, Pomoni-Papaioannou F and Alexopoulos A (1998) Biostratigraphical and sedimentological study of Upper Senonian—lower Eocene sediments of Tripolitza Platform in central Crete (Greece). *Cretaceous Research* **19**, 715–32.

Zulauf G, Dörr W, Marko L and Krahl J (2018) The late Eo-Cimmerian evolution of the External Hellenides: constraints from microfabrics and U-Pb detrital zircon ages of Upper Triassic (meta)sediments (Crete, Greece). *International Journal of Earth Sciences* **107**, 2859–2894. doi: 10.1007/s00531-018-1632-8.

Zulauf G, Kowalczyk G, Petschick R, Schwanz S and Krahl J (2002) The tectonometamorphic evolution of high-pressure low-temperature metamorphic rocks of eastern Crete, Greece: constraints from microfabrics, strain, illite crystallinity and paleostress. *Journal of Structural Geology* **24**, 1805–28.